Supporting Information for Publication:

Intra- and Interchain Interactions in $(Cu_{1/2}Au_{1/2})CN$, $(Ag_{1/2}Au_{1/2})CN$, and $(Cu_{1/3}Ag_{1/3}Au_{1/3})CN$ and Their Effect on One-, Two- and Three-Dimensional Order.

Simon J. Hibble[1]*, Ann M. Chippindale[2]*, Mohamed Zbiri[3], Nicholas H. Rees[4], Dean S. Keeble[5], Heribert Wilhelm[5], Stella d'Ambrumenil,[2,3] and David Seifert[6]

[1]Chemistry Teaching Laboratory, Department of Chemistry, University of Oxford, South Parks Road, Oxford, OX1 3PS, United Kingdom.

[2]Department of Chemistry, University of Reading, Whiteknights, Reading, RG6 6AD, United Kingdom.

[3]Institut Laue-Langevin, 71 avenue des Martyrs, Grenoble Cedex 9, 38042, France.

[4]Department of Chemistry, University of Oxford, Mansfield Road, Oxford, OX1 3TA, United Kingdom.

[5]Diamond Light Source, Harwell Campus, Oxfordshire, OX11 0DE, United Kingdom.

[6]School of Mathematics, Statistics and Physics, Herschel Building, Newcastle University,

Newcastle upon Tyne, NE1 7RU, United Kingdom

EMAIL ADDRESSES FOR CORRESPONDENCE:

simon.hibble@chem.ox.ac.uk

a.m.chippindale@rdg.ac.uk

S.1. Sample Preparation and Powder X-ray Diffraction Patterns of $(Cu_{1/2}Au_{1/2})CN$, $(Ag_{1/2}Au_{1/2})CN$ and $(Cu_{1/3}Ag_{1/3}Au_{1/3})CN$

Caution! Cyanide materials are toxic and must be handled with care. The addition of acid to soluble cyanides liberates highly toxic gaseous HCN. Both gaseous HCN and the aqueous washings, which contain HCN, were destroyed using alkaline hypochlorite.

All starting materials, LT-CuCN, AgCN, $AgNO_3$, AuCN and KCN, were used as supplied by Aldrich.

$(Cu_{1/2}Au_{1/2})CN$ was precipitated on addition of acid to a solution of the parent cyanides in aqueous potassium cyanide, as previously described.[1] LT-Copper cyanide (0.86 g, 9.6 mmol), gold cyanide (2.14 g, 9.6 mmol) and potassium cyanide (2.50 g, 38.4 mmol) were dissolved in 50 mL of deionised water. The resulting solution was vigorously stirred under a steady flow of nitrogen gas and 1 M nitric acid (40 mL, 40 mmol) was added to precipitate a pale-yellow solid. The precipitate was then washed in deionised water (500 mL), filtered and dried in air overnight. The sample was further dried prior to use by heating under vacuum at 80 °C for 14 h.

$(Ag_{1/2}Au_{1/2})CN$ was precipitated on addition of Ag^+ ions to a solution containing $[Au(CN)_2]^-$, as described previously.[1] A solution of $[Au(CN)_2]^-$ was prepared by dissolving gold cyanide (1.59 g, 7 mmol) with potassium cyanide (0.46 g, 7 mmol) in 50 mL of deionised water. A silver nitrate solution, prepared by dissolving $AgNO_3$ (1.2 g, 7 mmol) in 50 mL water, was added to the rapidly stirred $[Au(CN)_2]^-$ solution, immediately producing an off-white precipitate. After stirring for a further 10 minutes, the solid was filtered, rinsed well with water and dried as described above.

$(Cu_{1/3}Ag_{1/3}Au_{1/3})CN$ was precipitated on addition of acid to a solution of the parent cyanides in aqueous potassium cyanide, as previously described.[2] LT-Copper cyanide (0.179 g, 2 mmol), silver cyanide (0.268g, 2 mmol), gold cyanide (0.446 g, 2 mmol) and potassium cyanide (0.651 g, 10 mmol) were added to 8 mL of deionised water. The resulting solution was vigorously stirred under a steady flow of nitrogen gas and 1 M nitric acid (11 mL, 11 mmol) was added to precipitate a cream solid. The precipitate was then repeatedly washed in deionised water (20 mL aliquots), filtered and dried as described above.

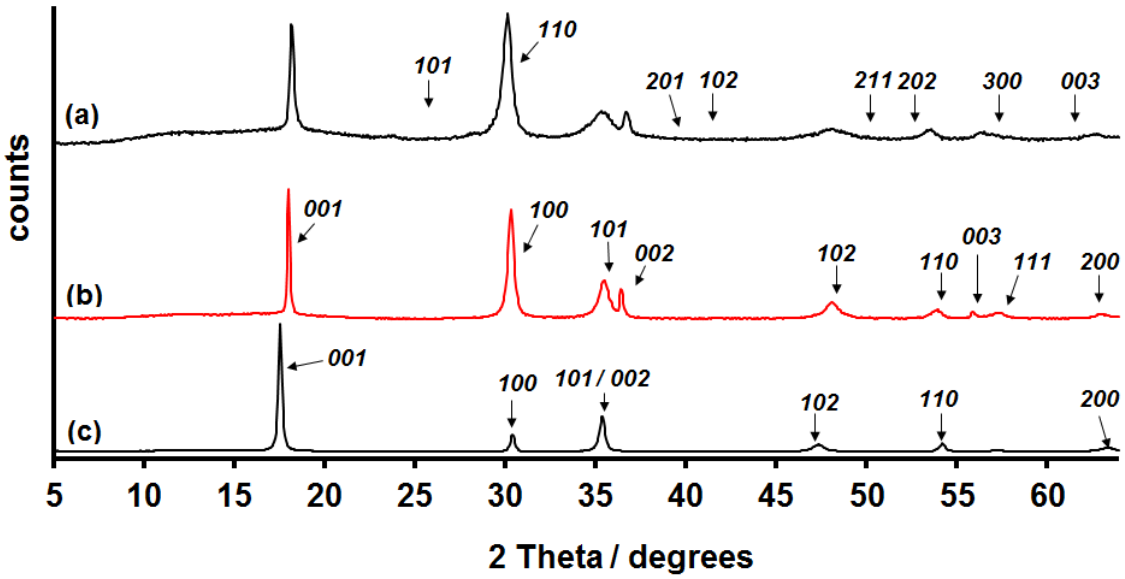

Figure S1a. PXRD patterns measured at room temperature of (a) HT-CuCN, (b) $(Cu_{1/2}Au_{1/2})CN$, and (c) AuCN and indexed on the basis of the AuCN structure type. AuCN has a hexagonal unit cell with a ~ 3.39 and c ~ 5.07 Å at room temperature.

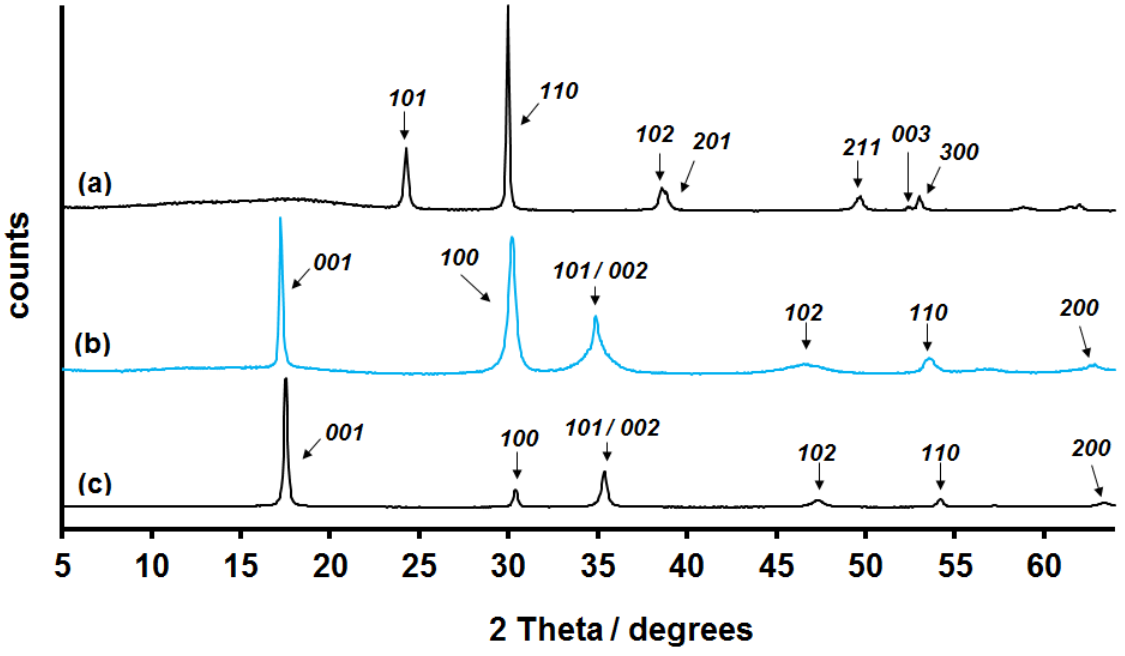

Figure S1b. PXRD patterns measured at room temperature of (a) AgCN, (b) $(Ag_{1/2}Au_{1/2})CN$ and (c) AuCN and indexed on the basis of the AuCN structure type. AuCN has a hexagonal unit cell with a ~ 3.39 and c ~ 5.07 Å at room temperature.

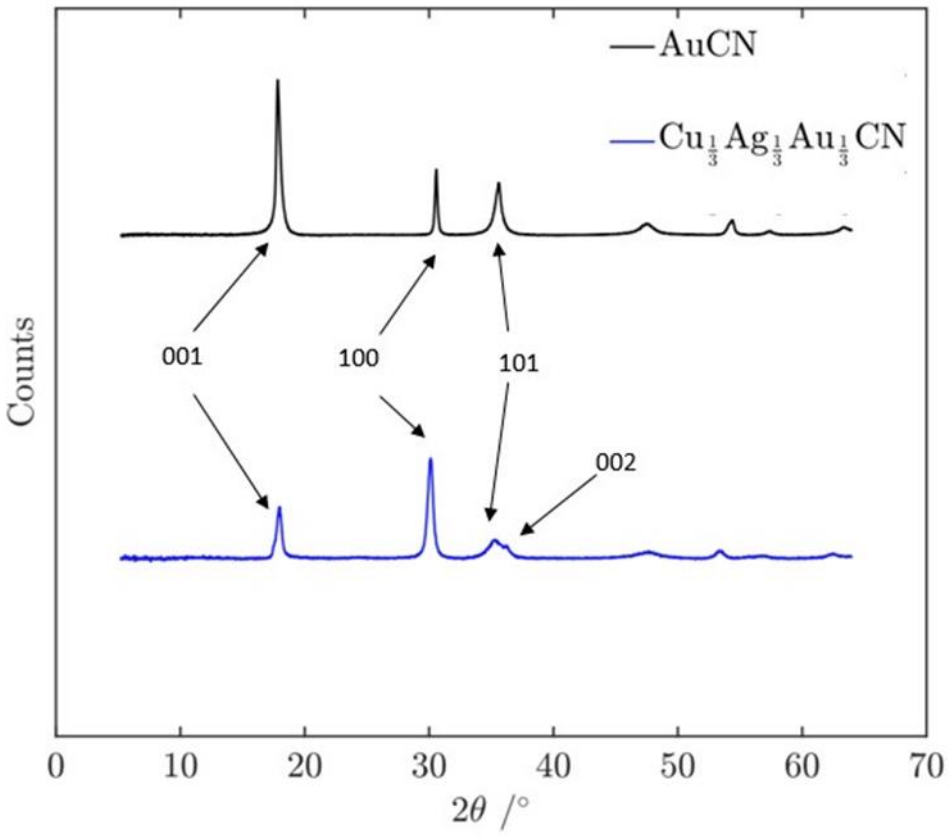

Figure S2. Powder X-ray diffraction patterns of AuCN and $(Cu_{1/3}Ag_{1/3}Au_{1/3})CN$ measured at room temperature and indexed on the basis of the AuCN structure type. AuCN has a hexagonal unit cell with a ~ 3.39 and c ~ 5.07 Å at room temperature.

References:

[1] Chippindale, A. M. ; Hibble, S. J. ; Bilbé, E.J. ; Marelli, E. ; Hannon, A.C. ; Allain, C. ; Pansu, R.; Hartl, F. Mixed Copper, Silver, and Gold Cyanides, $(M_xM'_{1-x})CN$: Tailoring Chain Structures to Influence Physical Properties. *J. Am. Chem. Soc*. **2012**, *134*, 16387 – 16400.

[2] d'Ambrumenil, S.; Zbiri, M.; Hibble, S. J.; Chippindale, A. M.; Keeble, D. S.; Wright, C. and Rees, N. H. Anomalous Thermal Expansion in One-Dimensional Transition-Metal Cyanides: Behavior of the Trimetallic Cyanide, $(Cu_{1/3}Ag_{1/3}Au_{1/3})CN$. *Phys Rev*., **2019**, *B100*, 174302 -1 – 174302 -13.

S.2. Mathematical Proof that Maximum Average Number of Heterometallic Nearest Neighbor Interactions on a Hexagonal Lattice is Four

Consider the regular hexagonal tiling of the plane, and suppose that each hexagon is colored either black or white. We investigate the average number, defined in a natural way, of oppositely colored neighboring tiles, and we show that this average cannot exceed 4.

Let *X* denote the set of all tiles. Given a two-coloring *c* of the tiling and a finite set $V \subseteq X$ we write $a_c(V)$ for the average number, taken over tiles $x \in V$, of tiles *y* adjacent to *x* such that $c(x) \neq c(y)$. For each tile $x \in V$ we define

$$u_c(x) = \limsup_{n\to\infty} a_c\big(V_n(x)\big) \qquad \text{and} \qquad l_c(x) = \liminf_{n\to\infty} a_c\big(V_n(x)\big),$$

where $V_n(x)$, $n \geq 0$, is the hexagonal region consisting of all tiles which are at distance at most *n* from *x*. We may interpret $u_c(x)$ as a local upper average and $l_c(x)$ as a local lower average number of unlike neighbors in the two-coloring *c* for the base point $x \in X$. By considering a two-coloring *c* in which there are concentric hexagonal regions of alternating averages and sufficiently rapidly growing thickness, we see that it is possible to have $u_c(x) > l_c(x)$ for some tiles $x \in X$. We say that a two-coloring *c* is *regular* if $u_c(x) = l_c(x)$ for all $x \in X$, and otherwise we call the two-coloring *irregular*. More specifically, we call a two-coloring *c weakly irregular* if $u_c(x) = l_c(x)$ for some $x \in X$ and $u_c(x) > l_c(x)$ for some $x \in X$, and we call the two-coloring *strongly irregular* if $u_c(x) > l_c(x)$ for all $x \in X$. If $u_c(x) = l_c(x)$ for some tile $x \in X$ then we denote the common value by $a_c(x)$, which we may interpret simply as the average number of unlike neighbors in the two-coloring *c* for the base point $x \in X$. Our first result shows that we have a dichotomy, and also that our notion of average is well adapted to the case of periodic colorings.

Proposition: *For any two-coloring c we have $u_c(x) = u_c(y)$ and $l_c(x) = l_c(y)$ for all $x, y \in X$. In particular, every two-coloring is either regular or strongly irregular. Furthermore, every periodic two-coloring c is regular and for all $x \in X$ we have $a_c(x) = a_c(Q)$, where $Q \subseteq X$ is any finite rhombus whose parallel translates generate the whole two-coloring c.*

Proof: Here and in what follows we view the regular hexagonal tiling as an infinite planar 6-regular graph *G* with vertex set $V(G) = X$. Let $E(G)$ be the set of edges in *G*. Given a two-coloring *c* of *X* we obtain a bipartite subgraph G_c of *G* with $V(G_c) = X$ and edge set $E(G_c) = \{xy \in E(G) : c(x) \neq c(y)\}$. For a vertex $x \in X$ we write $d_c(x)$ for the degree of *x* in the subgraph G_c. Letting $D_c(V) = \sum_{x\in V} d_c(x)$ for any finite set $V \subseteq X$ we have $a_c(V) = |V|^{-1} D_c(V)$. Moreover, for each $x \in X$ and $n \geq 0$ we have $V_n(x) = \{y \in X : d(x,y) \leq n\}$, where the distance $d(x,y)$ between two vertices $x, y \in X$ is given by the length of a shortest path in *G* between the two vertices. Now let $x \in X$. For a suitable subsequence we have $a_c(V_{n_k}(x)) \to u_c(x)$ as $k \to \infty$. Let $y \in X$ and set $r = d(x,y)$.

Since $V_n(x) \cup V_n(y) \subseteq V_{n+r}(x)$ for $n \geq 0$ and $V_{n-r}(x) \subseteq V_n(x) \cap V_n(y)$ for $n \geq r$, we see that for $n \geq r$ we have

$$\left|D_c\big(V_n(x)\big) - D_c\big(V_n(y)\big)\right| \leq D_c\big(V_{n+r}(x)\big) - D_c\big(V_{n-r}(x)\big).$$

Now

$$D_c\big(V_{n+r}(x)\big) \leq D_c\big(V_n(x)\big) + 6|V_{n+r}(x) \setminus V_n(x)|$$

and

$$D_c\big(V_{n-r}(x)\big) \geq D_c\big(V_n(x)\big) - 6|V_n(x) \setminus V_{n-r}(x)|,$$

and therefore

$$\left|a_c\big(V_n(x)\big) - a_c\big(V_n(y)\big)\right| \leq \frac{6}{|V_n(x)|}\left(|V_{n+r}(x)\setminus V_n(x)| + |V_n(x)\setminus V_{n-r}(x)|\right)$$

for all $n \geq r$. Since $|V_n(x)| = 3n(n+2)+1$, $n \geq 0$, it follows easily that $a_c(V_{n_k}(y)) \to u_c(x)$ as $k \to \infty$. In particular, $u_c(y) \geq u_c(x)$. By symmetry we obtain that $u_c(x) \geq u_c(y)$, and hence $u_c(x) = u_c(y)$, as required. Essentially the same argument shows that $l_c(x) = l_c(y)$ for all $x, y \in X$, and in particular every two-coloring c is either regular or strongly irregular.

Now suppose that the two-coloring c is periodic. Then there exist $m \geq 1$ and an $m \times m$ rhombus $Q \subseteq X$ whose parallel translates generate the whole two-coloring c. Fix $x \in X$ and note that $a_c(V_{km}(x)) = a_c(Q)$ for all $k \geq 1$. Given $n \geq m$ let $k \geq 1$ be such that $km \leq n < km + m$. Then

$$\left|a_c\big(V_n(x)\big) - a_c(Q)\right| \leq \Big(a_c\big(V_n(x)\big) + a_c(Q)\Big)\left(\frac{|V_{km+m}(x)|}{|V_{km}(x)|} - 1\right).$$

Since $a_c(V_n(x)) \leq 6$ for all $n \geq 0$ and moreover

$$\lim_{k\to\infty} \frac{|V_{km+m}(x)|}{|V_{km}(x)|} = 1,$$

it follows that $a_c(V_n(x)) \to a_c(Q)$ as $n \to \infty$. Hence the two-coloring c is regular and $a_c(x) = a_c(Q)$ for all $x \in X$. **Q.E.D.**

Given a two-coloring c of the hexagonal tiling we let $U(c) = u_c(x)$ and $L(c) = l_c(x)$, where $x \in X$ is any tile. These definitions make sense by the above Proposition, and we may interpret $U(c)$ as a global upper average and $L(c)$ a global lower average number of unlike neighbors in the two-coloring c. It is clear that $0 \leq L(c) \leq U(c) \leq 6$ for all two-colorings c, and by the Proposition we see that $U(c) = L(c)$ if and only if c is regular. Furthermore, it is easy to achieve $U(c) = L(c) = 0$ for instance by considering any two-coloring c which has only finitely many tiles colored in one of the two colors. By considering the regular two-coloring c involving infinite stripes of alternating color, we see that $U(c) = L(c) = 4$ is possible, too, and by considering a two-coloring c with growing

concentric regions which are alternately monochromatic and striped we may also achieve $U(c) = 4$ and $L(c) = 0$. Values strictly between 0 and 4 can also be achieved but, as the next result shows, values strictly greater than 4 cannot.

Theorem: *For any two-coloring c we have* $0 \leq L(c) \leq U(c) \leq 4$.

Proof: We need to prove only the upper bound on $U(c)$. We proceed as before and use the same notation as in the proof of the Proposition. Fix $x \in X$ and let $n \geq 0$. For $e \in E(G)$ we write $w_n(e)$ for the number of endpoints of e which lie in $V_n(x)$ and we let $E_n = \{e \in E(G) : w_n(e) \geq 1\}$. Furthermore, let $T_n(x)$ denote the set of all triangles in G which have at least two vertices lying in $V_n(x)$. Emanating from the corners of the hexagonal region $V_n(x)$ there are 6 edges $e \in E_n$ which satisfy $w_n(e) = 1$ and lie in no triangle $\Delta \in T_n(x)$. All other edges $e \in E_n$ lie in exactly $w_n(e)$ triangles $\Delta \in T_n(x)$. Thus

$$D_c\big(V_n(x)\big) = \sum_{e \in E_n} w_n(e) \mathbb{1}_{E(G_c)}(e) \leq 6 + \sum_{\Delta \in T_n(x)} |E(\Delta) \cap E(G_c)|.$$

Now the graph G_c, being bipartite, contains no triangles, so in particular $|E(\Delta) \cap E(G_c)| \leq 2$ for all $\Delta \in T_n$. Since $|T_n(x)| = 6n(n+1)$ it follows that

$$a_c\big(V_n(x)\big) = \frac{D_c(V_n(x))}{|V_n(x)|} \leq \frac{6 + 2|T_n(x)|}{3n(n+1)+1} = 4 + \frac{2}{3n(n+1)+1}.$$

Hence

$$U(c) = u_c(x) \leq \limsup_{n \to \infty} \left(4 + \frac{2}{3n(n+1)+1}\right) = 4.$$

Q.E.D.

S.3. Periodic Structural Models for $(M_{1/2}Au_{1/2})CN$ (M = Cu, Ag) (Models A – J) in Table 1

Note: Figures show packing in the metal layers only. All models have cyanide ordering with the carbon end of the ligand bound to gold.

Key as in Table 1: Au atoms, yellow spheres; Cu or Ag atoms, blue spheres

<u>Model A</u> *P*6/*mmm*{2}

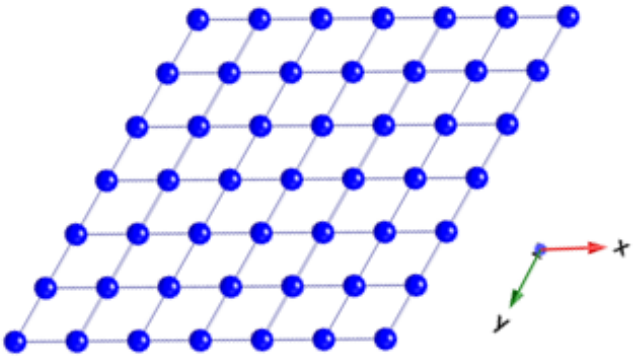

Metal Layer A

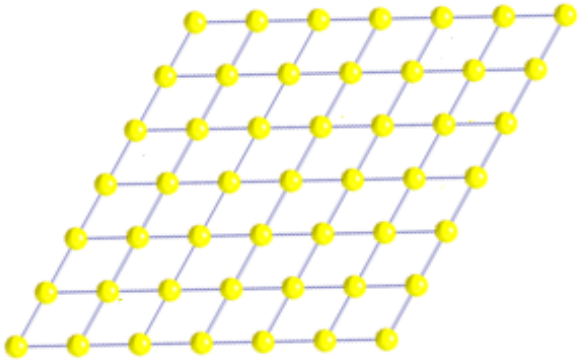

Metal Layer B

Model B ***Am2m*{8}**

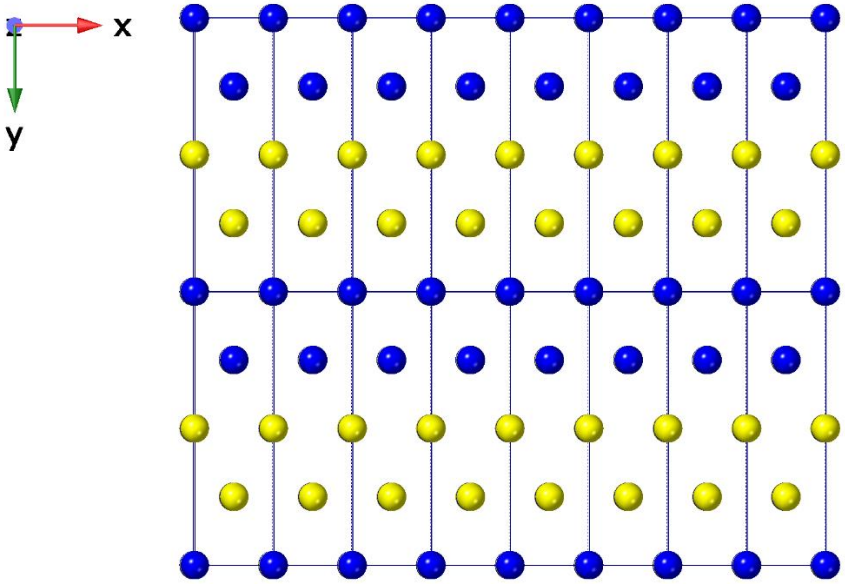

Model C ***Cmmm*** **{12}**

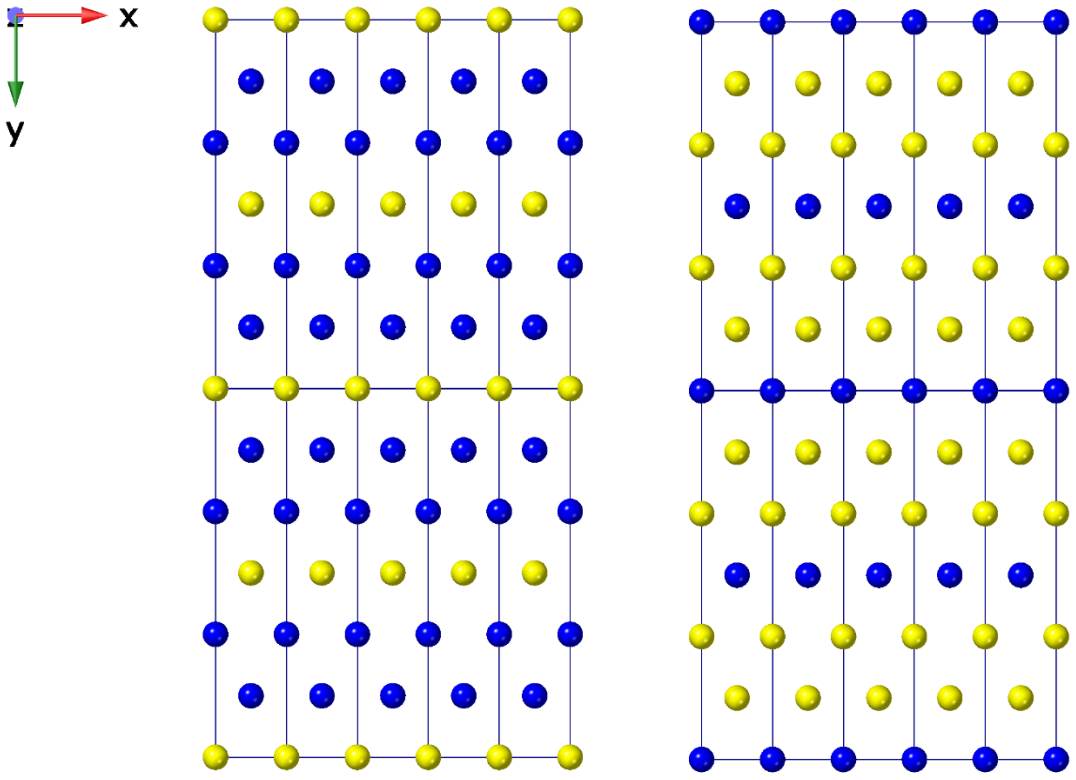

Metal Layer A:
Composition Cu_2Au_1

Metal Layer B:
Composition Cu_1Au_2

Model D ***Pmmm*{12}**

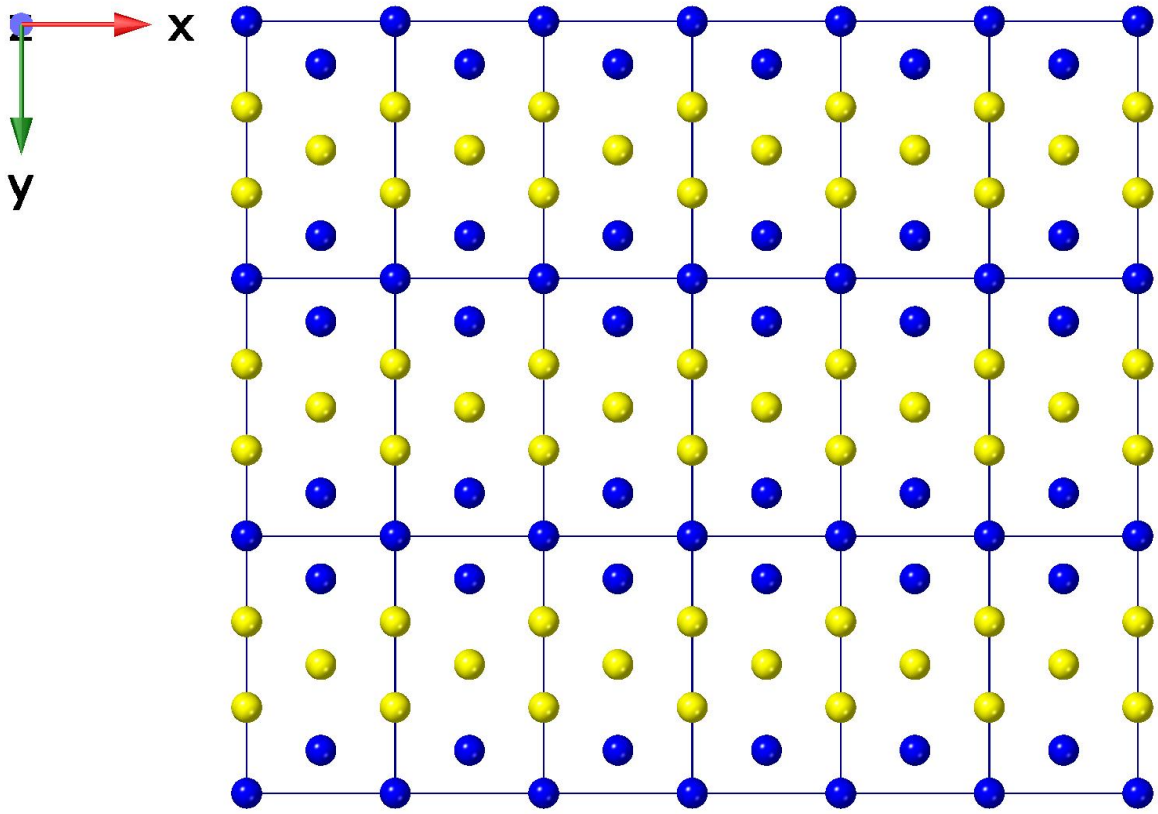

Model E ***Pmmm*{8}**

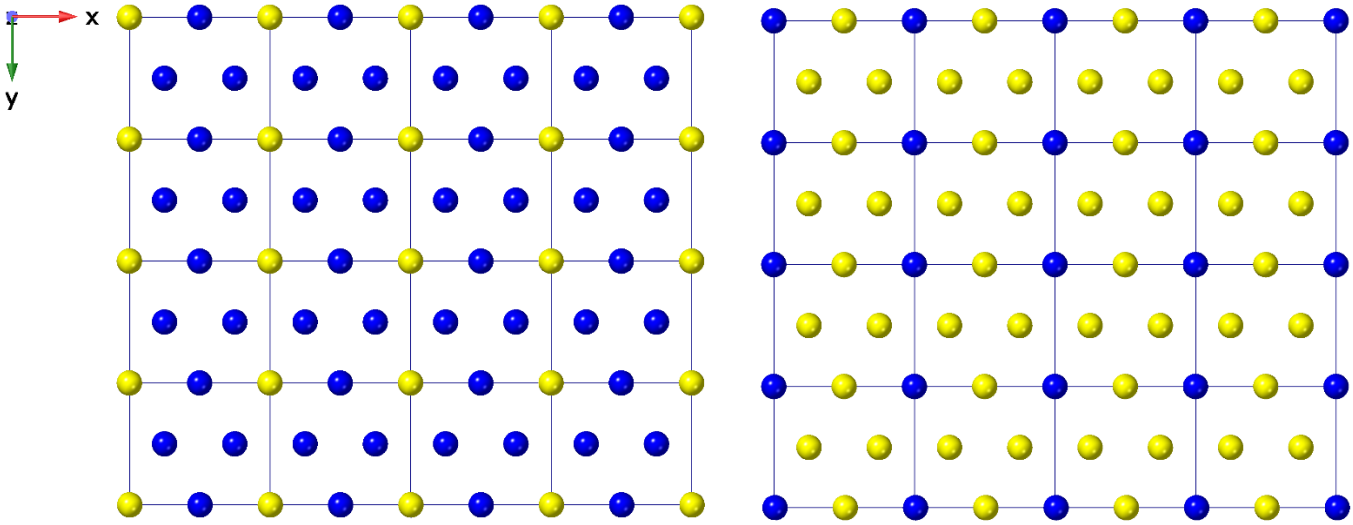

Metal Layer A:
Composition Cu_3Au_1

Metal Layer B:
Composition Cu_1Au_3

Model F *C*2/*m*{16}

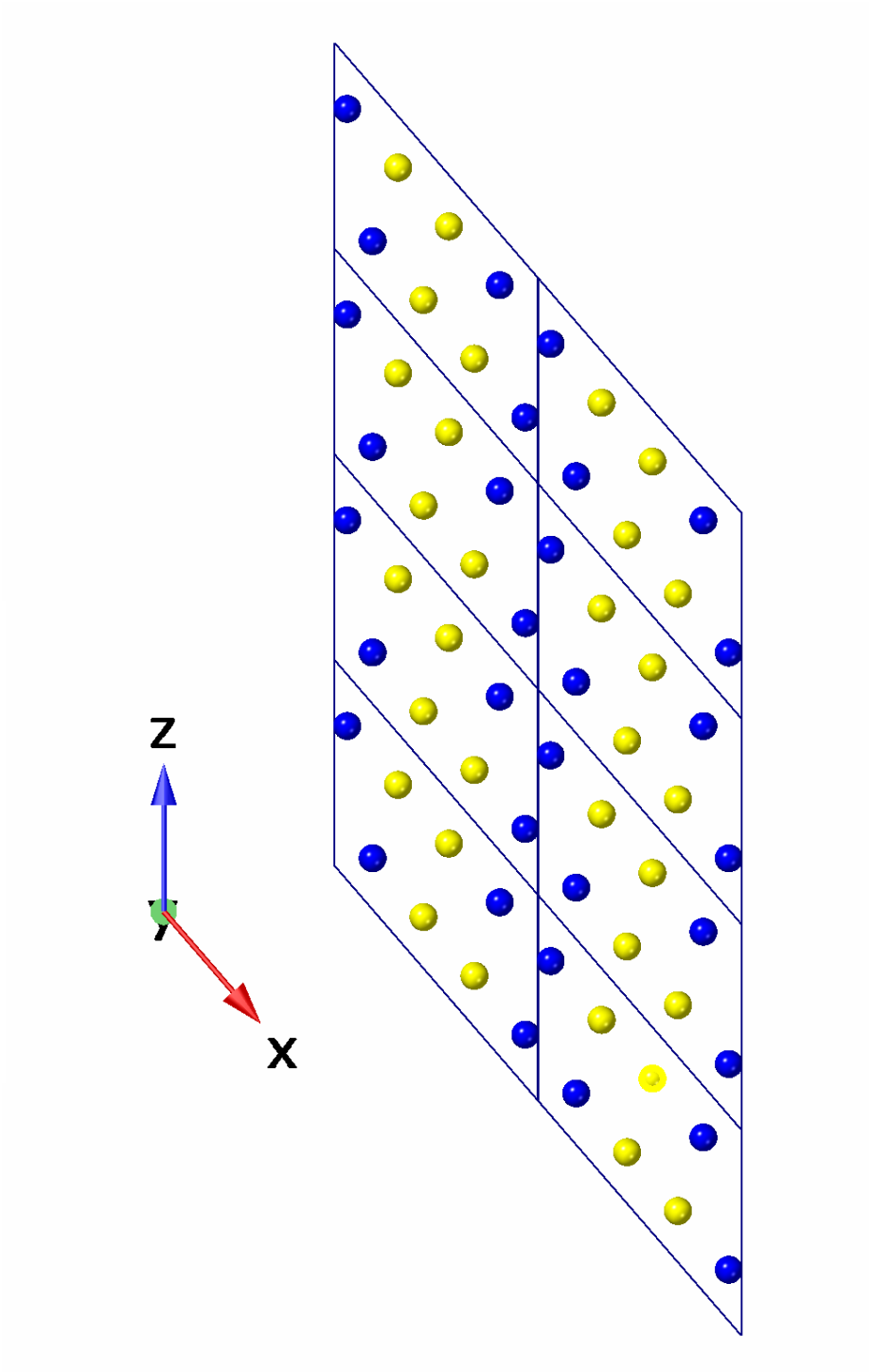

Model G ***Immm*** **{4}**

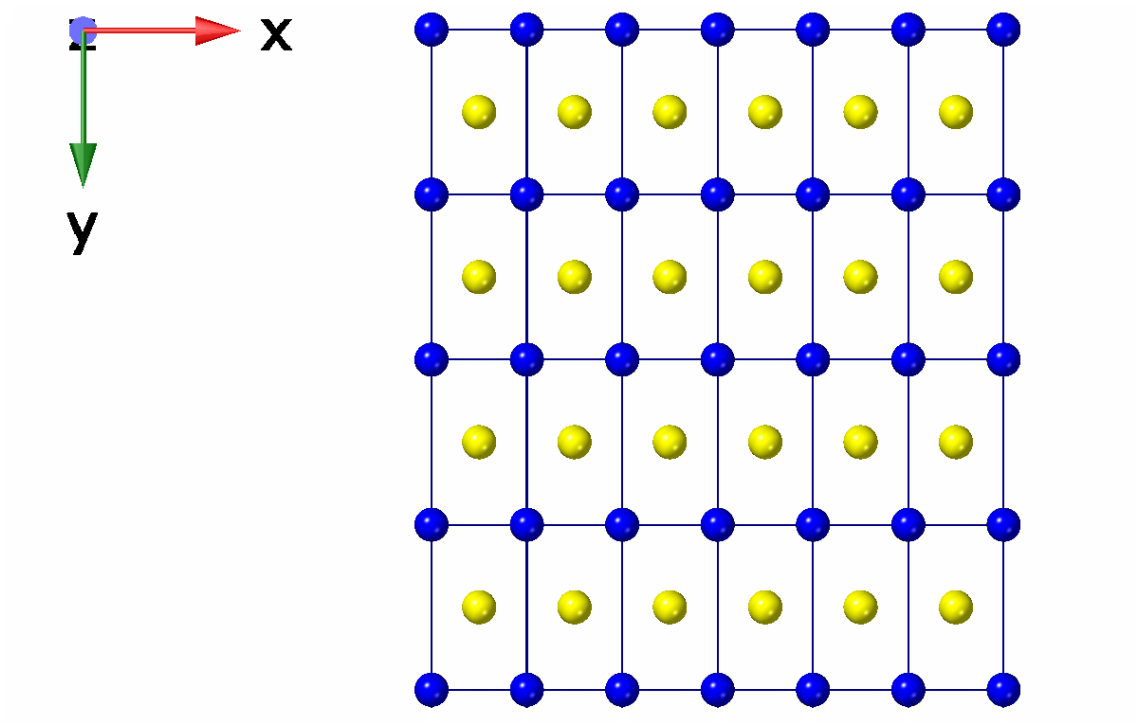

Model H ***Pmnm*** **{12}**

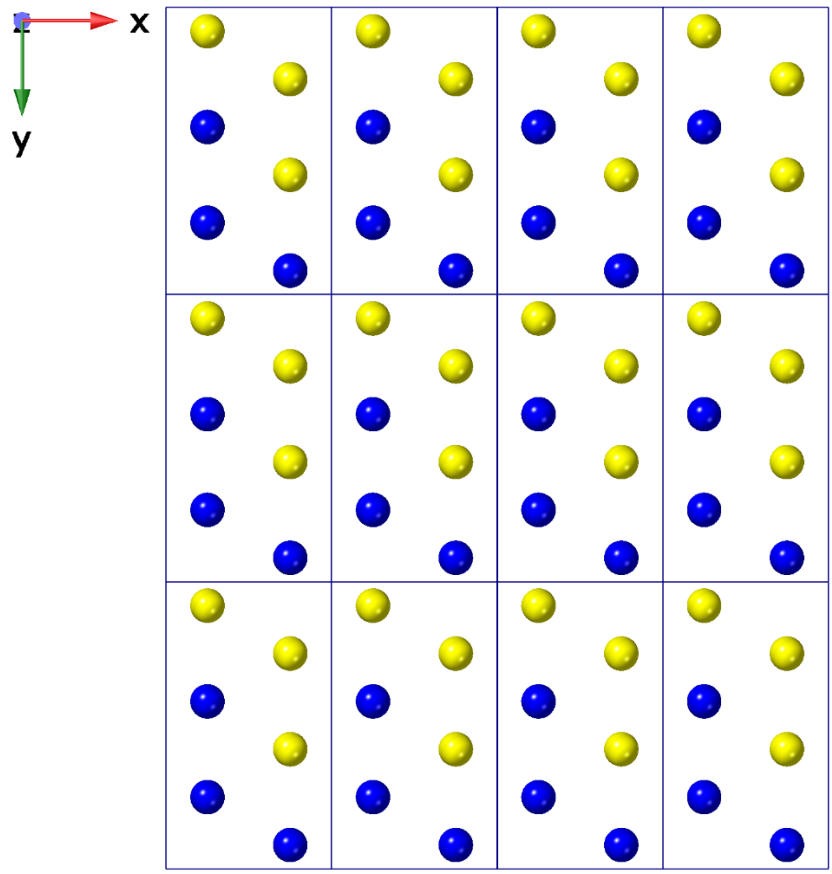

Model I ***Amam*{8}**

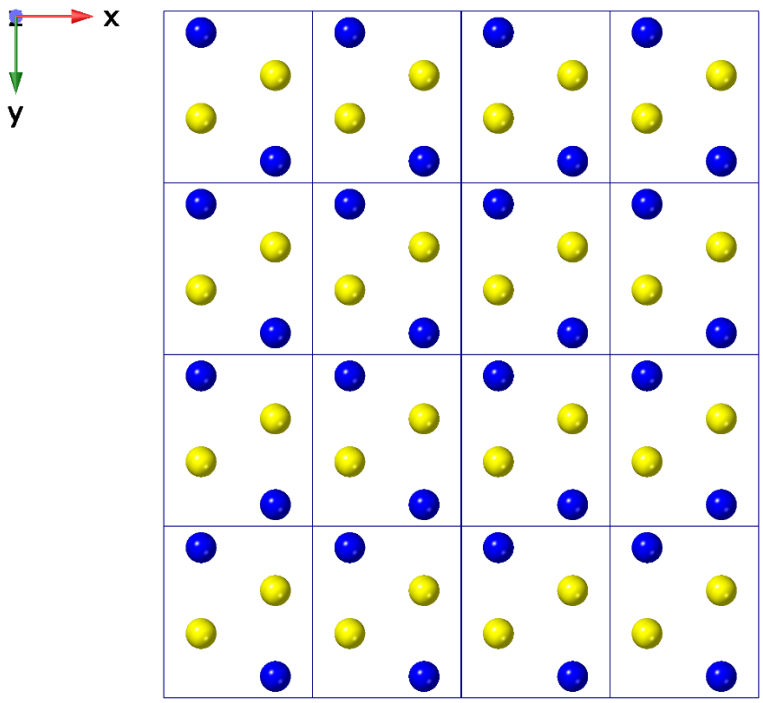

Model J ***P*6/*mmm*{6}**

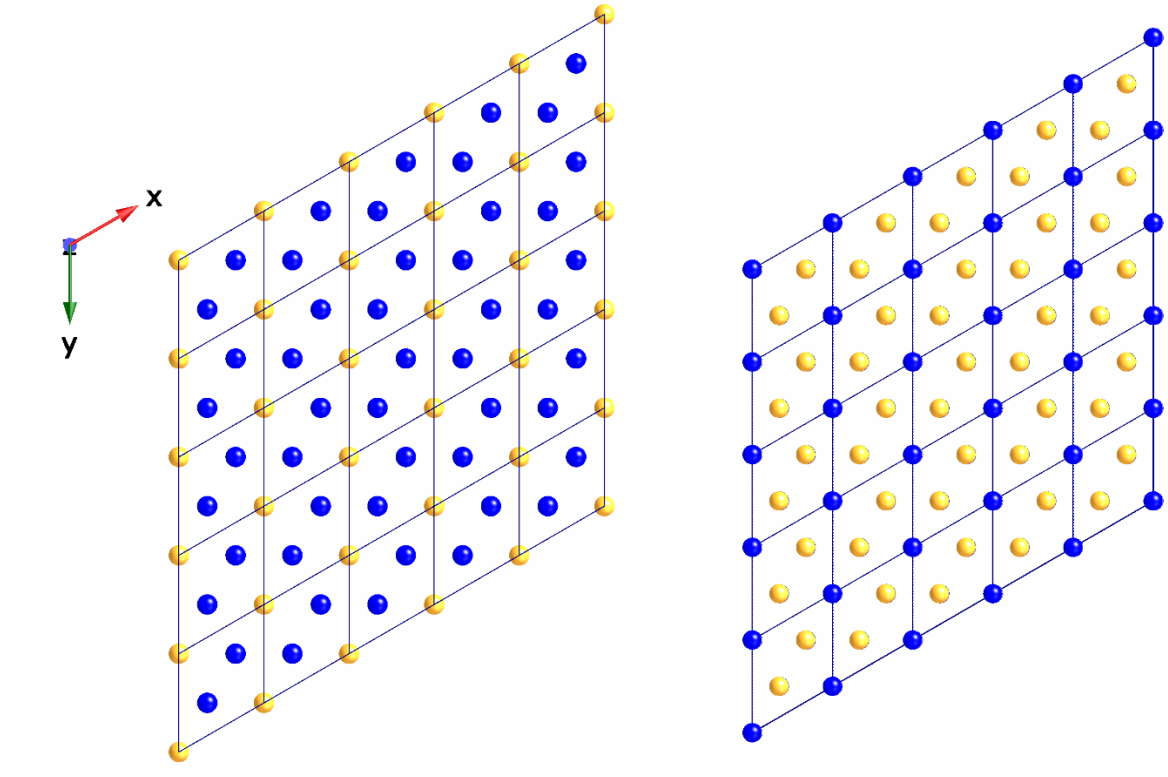

Metal Layer A:
Composition Cu_2Au_1

Metal Layer B:
Composition Cu_1Au_2

S.4. Total Energy Calculations for $(Cu_{1/2}Au_{1/2})CN$ and $(Ag_{1/2}Au_{1/2})CN$

DFT-based calculations were performed to investigate the relative energetic stabilities of several models (**A** – **J**) of $(M_{1/2}Au_{1/2})CN$ (M = Cu, Ag).

Calculations were carried out first without approximating possible weak interactions (aurophilic and/or argentophilic), then two DFT-based van der Waals' approaches were considered. The three calculation types are labelled no-vdW, vdW-1 and vdW-2, respectively.

Calculated energies are negative. In the following tables, by "scaled" energy it is meant that the lowest energy is taken as a reference: $E(scaled) = |E_0| - |Ei|$; where E_0 is the lowest energy per formula unit of a given structure, and Ei is the energy per formula unit of each of the model structures (i = **A** – **J**).

The energy differences between some structural models are very small, so more than one model could possibly be considered as being energetically stable with respect to the others.

Including vdW interactions does not alter the stability of the model structures with respect to each other.

The effect of interchanging C and N atoms in the metal-cyanide chains is also explored. Interchanging the C and N atoms does not alter the stability of the model structures with respect to each other. However, **the bonding sense –NC–Au–C≡N–M– is found to be energetically more stable than –CN–Au–N≡C–M–.**

Computational Details:

Total-energy calculations of the studied models were performed using the projector-augmented wave formalism [1, 2] of the Kohn-Sham density functional theory [3, 4] within the generalized gradient approximation (GGA), implemented in the Vienna *ab-initio* simulation package (VASP) [5]. [Note: Relativistic effects are included in the construction of the projector augmented wave-based pseudopotentials used in the VASP code [1, 2, 5, 6]. VASP performs a fully relativistic calculation for the core-electrons and treats valence electrons in a scalar relativistic approximation.]
The GGA was formulated by the Perdew–Burke–Ernzerhof (PBE) density functional [7]. The Gaussian broadening technique was adopted and all results were well converged with respect to *k*-mesh and energy cutoff for the plane-wave expansion. A plane-wave energy cutoff of 700 eV was used, and the integrations over the Brillouin zone were sampled using grids of k-points generated by the Monkhorst-pack method [8]. The break condition for the self-consistent field (SCF) loop was set to 10^{-8} eV. Given the weak and dispersive nature of the aurophilic and/or argentophilic effects, stemming from closed *d*-shell dispersive weak interactions (where applicable), they can be described by van der Waals' type interactions. Standard Kohn-Sham-based DFT lacks the description of static, long-ranged, dispersion forces [9]. Therefore, a vdW-type correction should be considered within the present DFT framework. In VASP, various vdW-based schemes, accounting for the London-like R^{-6} behavior, originating from nonlocal electron correlation [10, 11], are available. Two vdW approximations, based on the representative significance of their conceptual implementation, were explored. The first vdW approach is based on the Grimme method [12] (vdW-1). The second is a density functional where the non-local correlation functional approximately accounts for dispersion interactions [13, 14] - presently we adopt the one called optPBE-vdW [15] (vdW-2). The validity of such treatment can further be supported by other works in the literature [16-19].

References:

[1] G. Kresse, and D. Joubert, *Phys. Rev*. **B59**, 1758 (1999).
[2] A. Dal Corso, *Phys. Rev*. **B82**, 075116 (2010).
[3] P. Hohenberg and W. Kohn, *Phys. Rev.* **B136**, 864 (1964).
[4] W. Kohn and L. J. Sham, *Phys. Rev*. **A140**, 1133 (1965).
[5] G. Kresse, and J. Furthmüller, *Comput. Mater. Sci*. **6**, 15 (1996).
[6] G. Kresse and J. Furthmüller, *Phys. Rev*. **B54**, 11169 (1996)
[7] J. P. Perdew, K. Burke, and M. Ernzerhof, *Phys. Rev. Lett.* **77**, 3865 (1996).
[8] H. J. Monkhorst, and J.D. Pack, *Phys. Rev*. **B13**, 5188 (1976).
[9] S. F. Sousa, P. A. Fernandes and M. J. Ramos, *J. Phys. Chem. A* **111**, 10439 (2007).
[10] J. Li and P. Pyykkö, *Chem. Phys. Lett*. **197**, 586 (1992).
[11] P. Pyykkö and F. Mendizabal, *Chem. Eur. J*. **3**, 1458 (1997).
[12] S. Grimme, J. *Comp. Chem. 27*, 1787 (2006).
[13] M. Dion, H. Rydberg, E. Schröder, D. C. Langreth, and B. I. Lundqvist, *Phys. Rev. Lett*. **92**, 246401 (2004).
[14] G. Roman-Pérez, J. M. Soler, *Phys. Rev. Lett.* **103**, 096102 (2009).
[15] J. Klimes, D. R. Bowler, and A. Michaelides, *J. Phys.: Condens. Matt*. **22**, 022201 (2010).
[16] M. Calleja, A. L. Goodwin and M. T. Dove, *J. Phys.: Condens. Matter*. **20**, 255226 (2008).

[17] A. L. Goodwin, M. Calleja, M. J. Conterio, M. T. Dove, J. S. O. Evans, D. A. Keen, L. Peters and M. G. Tucker, *Science* **319**, 794 (2008).
[18] B. Vlaisavljevich, J. Huck, Z. Hulvey, K. Lee, J. A. Mason,
J. B. Neaton, J. R. Long, C. M. Brown, D. Alfè, A. Michaelides,
and B. Smit, *J. Phys. Chem. A* **121**, 4139 (2017).
[19] E. Andris, P. C. Andrikopoulos, J. Schulz, J Turek, A. Ruzicka, J. Roithova and L. Rulisek, *J. Am. Chem. Soc.* 2018, 140, 6, 2316 (2018).

Table S1. Scaled energies for $(Cu_{1/2}Au_{1/2})CN$, i.e., the energy difference (per $(Cu_{1/2}Au_{1/2})CN$ formula unit) between each model (A – J) and model (J) with chain ordering in the sense –N≡C–Au–C≡N–Cu–.

$(Cu_{1/2}Au_{1/2})CN$ with chain ordering in the sense –N≡C–Au–C≡N–Cu–					
Structural Model	Space group	F.U./U.C. [$]	ΔE/F.U.[#] / eV		
			no vdW	vdW-1	vdW-2
A	*P*6/*mmm*{2}	2	0.0472	0.0713	0.0461
B	*Am*2*m*{8}	8	0.0251	0.0425	0.0238
C	*Cmmm*{12}	12	0.0199	0.0324	0.0183
D	*Pmmm*{12}	12	0.0189	0.0320	0.0174
E	*Pmmm*{8}	8	0.0177	0.0259	0.0160
F	*C*2/*m*{16}	16	0.0161	0.0269	0.0145
G	*Immm*{4}	4	0.0085	0.0118	0.0065
H	*Pmnm*{12}	12	0.0078	0.0097	0.0057
I	*Amam*{8}	8	0.0077	0.0101	0.0056
J	P6/*mmm*{6}	6	0.0000	0.0000	0.0000

[$] F.U./U.C. Formula Unit per Unit Cell.

[#] ΔE/F.U. Energy per Formula Unit

Note: Without applying a vdW correction, the most stable model is **J** (P6/*mmm*{6}) and the least stable is **A** (P6/*mmm*{2}). This conclusion does not change when vdW effects are included using the two different approximations, vdW-1 and vdW-2.

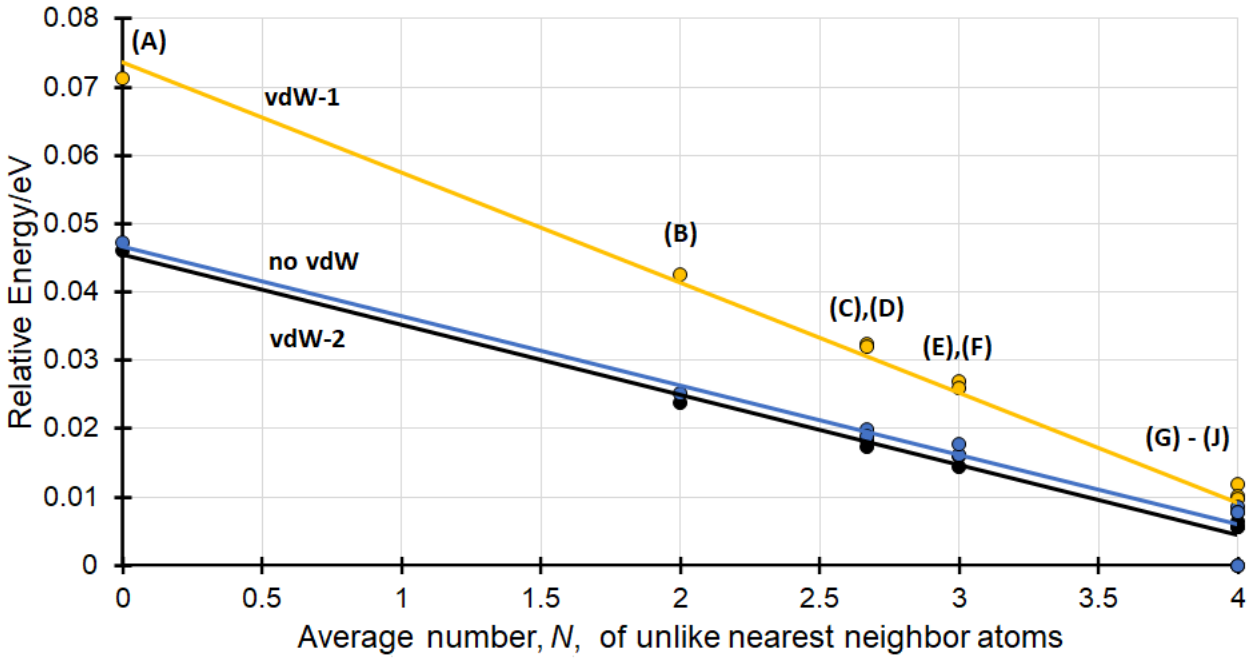

Figure S3. The scaled energies per formula unit of $(Cu_{1/2}Au_{1/2})CN$ for the different crystallographic models **(A – J)** as a function of number of nearest-neighbor heterometallic atoms calculated using the three DFT schemes: no-vdW (blue), vdW-1(orange) and vdW-2 (black) (Table S1).

Table S2. Scaled energies for $(Ag_{1/2}Au_{1/2})CN$, i.e., the energy difference (per $(Ag_{1/2}Au_{1/2})CN$ formula unit) between each model (A – J) and model (I) with chain ordering in the sense –N≡C–Au–C≡N–Ag–.

$(Ag_{1/2}Au_{1/2})CN$ with chain ordering in the sense –N≡C–Au–C≡N–Ag–					
Structural Model	Space group	F.U./U.C.[$]	ΔE/F.U.[#] / eV		
			no vdW	vdW-1	vdW-2
A	*P*6/*mmm*{2}	2	0.5423	0.0461	0.0426
B	*Am*2*m*{8}	8	0.0155	0.0198	0.0159
C	*Cmmm*{12}	12	0.0114	0.0143	0.0116
D	*Pmmm*{12}	12	0.0097	0.0130	0.0101
E	*Pmmm*{8}	8	0.0108	0.0118	0.0109
F	*C*2/*m*{16}	16	0.0072	0.0098	0.0074
G	*Immm*{4}	4	0.0008	0.0012	0.0008
H	*Pmnm*{12}	12	0.0003	0.0000	0.0003
I	*Amam*{8}	8	0.0000	0.0000	0.0000
J	P6/*mmm*{6}	6	0.0019	0.0007	0.0018

[$] F.U./U.C. Formula Unit per Unit Cell.

[#] ΔE/F.U. Energy per Formula Unit

Note: In the absence of a vdW correction, the most stable model is (**I)** (*Amam*{8}) and the least stable is (**A)** (*P*6/*mmm*{2}). This does not change when including vdW effects using the two different approximations, vdW-1 and vdW-2. In addition, applying vdW interactions to model (**A)** stablilizes the structure greatly.

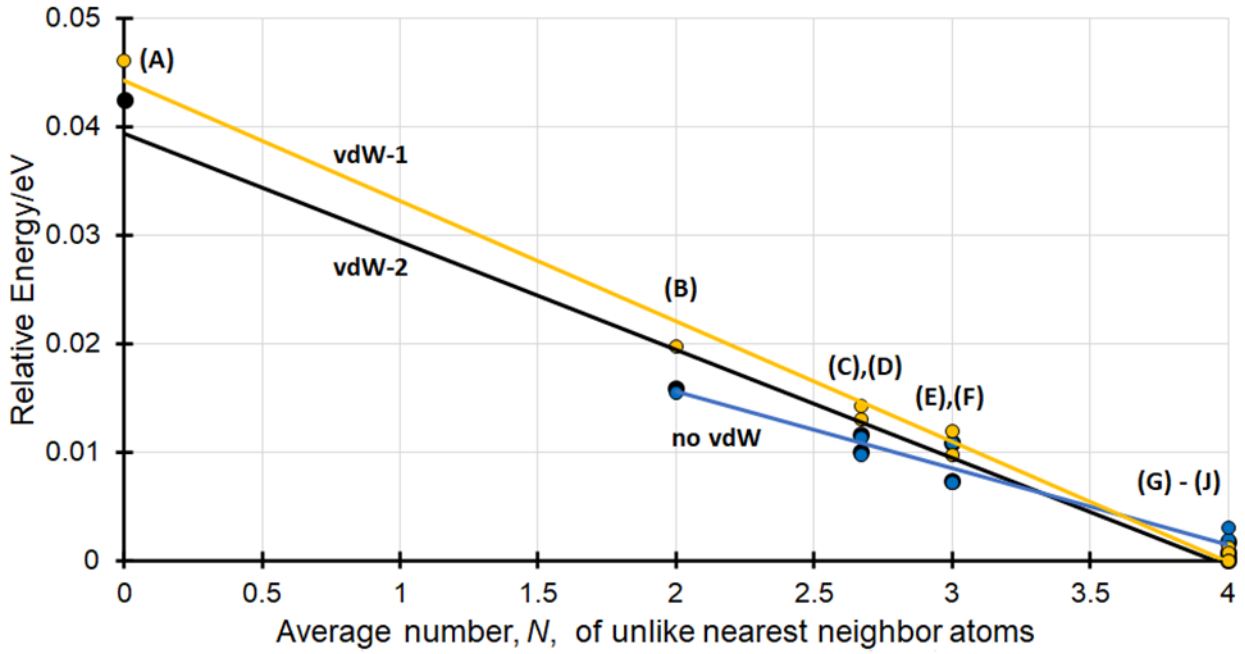

Figure S4. The scaled energies per formula unit of $(Ag_{1/2}Au_{1/2})CN$ different crystallographic models **(A – J)** as a function of number of nearest-neighbor heterometallic atoms calculated using the three DFT schemes: no-vdW (blue), vdW-1(orange) and vdW-2 (black). (Table S2).

Note: The relative energy of $(Ag_{1/2}Au_{1/2})CN$ with $N = 0$ calculated without van der Waals' interactions is extremely high (+~0.54 eV) and the point is therefore excluded from the plot.

Table S3. Comparison of total energies per formula unit for $(Cu_{1/2}Au_{1/2})CN$ on interchanging C and N atoms along the chains.

$(Cu_{1/2}Au_{1/2})CN$									
Total Energies per $(Cu_{1/2}Au_{1/2})CN$ formula unit /eV									
	no vdW			vdW-1			vdW-2		
Structural Model	-NC-Au-CN-	-CN-Au-NC-	ΔE	-NC-Au-CN-	-CN-Au-NC-	ΔE	-NC-Au-CN-	-CN-Au-NC-	ΔE
A	-20.0214	-19.6976	-0.3244	-20.8870	-20.5541	-0.3329	-14.2608	-13.9424	-0.3184
B	-20.0435	-19.7140	-0.3295	-20.9158	-20.5837	-0.3321	-14.2831	-13.9601	-0.3230
C	-20.0487	-19.7164	-0.3323	-20.9258	-20.5928	-0.3333	-14.2886	-13.9628	-0.3258
D	-20.0496	-19.7175	-0.3321	-20.9263	-20.5935	-0.3328	-14.2895	-13.9640	-0.3255
E	-20.0509	-19.7169	-0.3340	-20.9324	-20.5985	-0.3339	-14.2909	-13.9633	-0.3276
F	-20.0525	-19.7191	-0.3334	-20.9313	-20.5983	-0.3330	-14.2925	-13.9657	-0.3268
G	-20.0601	-19.7227	-0.3374	-20.9465	-20.6122	-0.3328	-14.3004	-13.9696	-0.3308
H	-20.0608	-19.7235	-0.3371	-20.9486	-20.6142	-0.3344	-14.3012	-13.9704	-0.3308
I	-20.0609	-19.7235	-0.3374	-20.9481	-20.6138	-0.3343	-14.3013	-13.9705	-0.3308
J	-20.0686	-19.7336	-0.3350	-20.9583	-20.6260	-0.3383	-14.3069	-13.9784	-0.3276
	Average of ΔE		**-0.3333(40)**	**Average of ΔE**		**-0.3338(18)**	**Average of ΔE**		**-0.3267(39)**

The bonding sense –N≡C–Au–C≡N–Cu– in the chains is found to be energetically more stable than –C≡N–Au–N≡C–Cu–, with or without the inclusion of vdW interactions.

Table S4. Comparison of total energies per formula unit for $(Ag_{1/2}Au_{1/2})CN$ on interchanging C and N atoms along the chains.

$(Ag_{1/2}Au_{1/2})CN$									
Total Energies per $(Ag_{1/2}Au_{1/2})CN$ formula unit /eV									
	no vdW			vdW-1			vdW-2		
Model	-NC-Au-CN-	-CN-Au-NC-	ΔE	-NC-Au-CN-	-CN-Au-NC-	ΔE	-NC-Au-CN-	-CN-Au-NC-	ΔE
A	-18.8181	-19.0700	+0.2519	-20.2882	-20.0303	-0.2579	-13.4758	-13.2314	-0.2444
B	-19.3449	-19.0813	-0.2636	-20.3146	-20.0458	-0.2688	-13.5026	-13.2445	-0.2581
C	-19.3491	-19.0821	-0.2670	-20.3201	-20.0493	-0.2708	-13.5069	-13.2456	-0.2613
D	-19.3506	-19.0831	-0.2675	-20.3213	-20.0500	-0.2713	-13.5084	-13.2467	-0.2617
E	-19.3496	-19.0816	-0.2680	-20.3225	-20.0513	-0.2712	-13.5076	-13.2453	-0.2609
F	-19.3532	-19.0839	-0.2696	-20.3245	-20.0521	-0.2724	-13.5111	-13.2477	-0.2637
G	-19.3596	-19.0851	-0.2681	-20.3331	-20.0575	-0.2756	-13.5176	-13.2494	-0.2682
H	-19.3601	-19.0856	-0.2745	-20.3343	-20.0586	-0.2757	-13.5182	-13.2500	-0.2682
I	-19.3604	-19.0858	-0.2746	-20.3343	-20.0586	-0.2763	-13.5185	-13.2502	-0.2683
J	-19.3585	-19.0847	-0.2738	-20.3336	-20.0586	-0.2750	-13.5167	-13.2491	-0.2696
	Average of $\Delta E^{\S}$		**-0.2696(44)**	**Average of ΔE**		**-0.2715(54)**	**Average of ΔE**		**-0.2624(75)**

The bonding sense –N≡C–Au–C≡N–Ag– in the chains is found to be energetically more stable than –C≡N–Au–N≡C–Ag–, with or without the inclusion of vdW interactions. [The only exception is model **A** in the absence of a vdW correction].

$\Delta E^{\S}$ ignoring result for model (**A)**

Table S5. Calculated Energies per ($M_{1/2}Au_{1/2}$)CN Formula Unit for the Models for ($Cu_{1/2}Au_{1/2}$)CN and ($Ag_{1/2}Au_{1/2}$)CN Relative to the Model with the Lowest Energy used in Figure 4.

Structural Model	Space group	No. heterometallic nearest neighbors in sheet, *N*	($Cu_{1/2}Au_{1/2}$)CN Relative Energy/eV [§]	($Ag_{1/2}Au_{1/2}$)CN Relative Energy/eV [§]
A	*P*6/*mmm*{2}	0	0.0461	0.0426
B	*Am*2*m*{8}	2	0.0238	0.0159
C	*Cmmm* {12}	2⅔	0.0183	0.0116
D	*Pmmm*{12}	2⅔	0.0174	0.0101
E	*Pmmm*{8}	3	0.016	0.0109
F	*C*2/*m*{16}	3	0.0145	0.0074
G	*Immm* {4}	4	0.0065	0.0008
H	*Pmnm* {12}	4	0.0057	0.0003
I	*Amam*{8}	4	0.0056	0
J	*P*6/*mmm*{6}	4	0	0.0018

[§]Values from DFT Calculations using vdW-2.

S.5. Details of Selected Structural Models for $(Cu_{1/2}Au_{1/2})CN$ and $(Ag_{1/2}Au_{1/2})CN$

Table S6. Model A, Homometallic Layers
The *P*/6*mmm*{2} model for $(Cu_{1/2}Au_{1/2})CN$ at 100 K with $[–NC–Au–CN–Cu]_n$ ordered chains.
Hexagonal unit cell: *a* = 3.359, *c* = 9.914 Å

Atom	*x*	*y*	*z*	Wyckoff position
Au	0	0	1/2	1*b*
Cu	0	0	0	1*a*
C	0	0	0.3004	2*e*
N	0	0	0. 1842	2*e*

Table S7. Model A, Homometallic Layers
The *P*/6*mmm*{2} model for $(Ag_{1/2}Au_{1/2})CN$ at 100 K with $[–NC–Au–CN–Ag]_n$ ordered chains.
Hexagonal unit cell: *a* = 3.375, *c* = 10.366 Å

Atom	*x*	*y*	*z*	Wyckoff position
Au	0	0	1/2	1*b*
Ag	0	0	0	1*a*
C	0	0	0.3085	2*e*
N	0	0	0.1970	2*e*

Table S8. Model G
The *Immm*{4} model for $(Cu_{1/2}Au_{1/2})CN$ at 100 K with $[–NC–Au–CN–Cu]_n$ ordered chains.
Orthorhombic unit cell: *a* = 3.359, *b* = 5.818 and *c* = 9.914 Å

Atom	*x*	*y*	*z*	Wyckoff position
Au	0	0	0	2*a*
Cu	0	0	1/2	2*c*
C	0	0	0.1996	4*i*
N	0	0	0.6842	4*i*

Table S9. Model G
The *Immm*{4} model for $(Ag_{1/2}Au_{1/2})CN$ at 100 K with $[–NC–Au–CN–Ag]_n$ ordered chains.
Orthorhombic unit cell: *a* = 3.3752, *b* = 5.8460 and *c* = 10.3660 Å

Atom	*x*	*y*	*z*	Wyckoff position
Au	0	0	0	2*a*
Ag	0	0	1/2	2*c*
C	0	0	0.1915	4*i*
N	0	0	0.3030	4*i*

Table S10. Model I
The *Amam*{8} model for $(Cu_{1/2}Au_{1/2})CN$ at 100 K with $[–NC–Au–CN–Cu]_n$ ordered chains.
Orthorhombic unit cell: *a* = 5.818, *b* = 6.718 and *c* = 9.914 Å

Atom	*x*	*y*	*z*	Wyckoff position
Au	1/4	0.125	1/2	4*c*
Cu	1/4	0.125	0	4*c*
C	1/4	0.125	0.3004	8*g*
N	1/4	0.125	0.1842	8*g*

Table S11. Model I
The *Amam*{8} model for $(Ag_{1/2}Au_{1/2})CN$ at 100 K with $[–NC–Au–CN–Ag]_n$ ordered chains.
Orthorhombic unit cell: *a* = 5.846, *b* = 6.7504 and *c* = 10.366 Å

Atom	*x*	*y*	*z*	Wyckoff position
Au	1/4	0.125	1/2	4*c*
Ag	1/4	0.125	0	4*c*
C	1/4	0.125	0.6915	8*g*
N	1/4	0.125	0.1970	8*g*

Table S12. Model J
The *P*/6*mmm*{6} model for ($Cu_{1/2}Au_{1/2}$)CN at 100 K with [–NC–Au–CN–Cu]$_n$ ordered chains.
Hexagonal unit cell: *a* = 5.818, *c* = 9.914 Å

Atom	*x*	*y*	*z*	Wyckoff position
Au1	0	0	1/2	1*b*
Au2	1/3	2/3	0	2*c*
Cu1	0	0	0	1*a*
Cu2	1/3	2/3	1/2	2*d*
C1	0	0	0.3004	2*e*
C2	1/3	2/3	0.1986	4*h*
N1	0	0	0.1842	2*e*
N2	1/3	2/3	0.3158	4*h*

Table S13. Model J
The *P*/6*mmm*{6} model for ($Ag_{1/2}Au_{1/2}$)CN at 100 K with [–NC–Au–CN–Ag]$_n$ ordered chains.
Hexagonal unit cell: *a* = 5.846, *c* = 10.366 Å

Atom	*x*	*y*	*z*	Wyckoff position
Au1	0	0	1/2	1*b*
Au2	1/3	2/3	0	2*c*
Ag1	0	0	0	1*a*
Ag2	1/3	2/3	1/2	2*d*
C1	0	0	0.6915	2*e*
C2	1/3	2/3	0.1915	4*h*
N1	0	0	0.1970	2*e*
N2	1/3	2/3	0.6970	4*h*

S.6. Details of Structural Models for (Cu1/3Ag1/3Au1/3)CN (models K – N) in Table 2

Table S14. Model K
The *P6mm* model for $(Cu_{1/3}Ag_{1/3}Au_{1/3})CN$ at 100 K with $[Cu–NC–Ag–NC–Au–CN]_n$ ordered chains.
Hexagonal unit cell: *a* = 3.39, *c* = 15.01 Å [ref 16]

Atom	*x*	*y*	*z*	Wyckoff position
Au1	0	0	0	1*a*
Ag1	0	0	0.6580	1*a*
Cu1	0	0	0.3260	1*a*
C1	0	0	0.1301	1*a*
C2	0	0	0.5218	1*a*
C3	0	0	0.8699	1*a*
N1	0	0	0.2058	1*a*
N2	0	0	0.4461	1*a*
N3	0	0	0.7942	1*a*

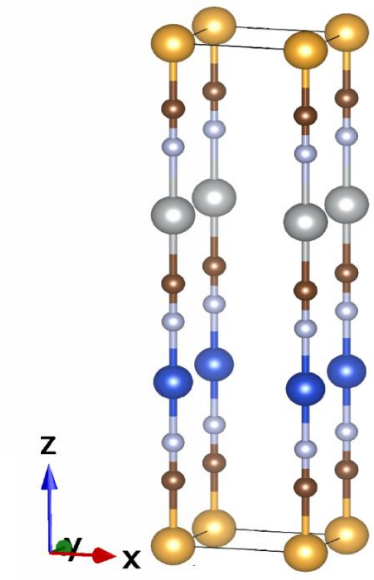

Figure S5. Model K. Key: Au atoms, yellow spheres; Ag atoms, silver spheres; Cu atoms, blue spheres; C atoms, brown spheres and N atoms, gray spheres.

Table S15. Model L
The *R*3*m* model for $(Cu_{1/3}Ag_{1/3}Au_{1/3})CN$ at 100 K with $[Cu–NC–Ag–NC–Au–CN]_n$ ordered chains.
Hexagonal unit cell: *a* = 5.87, *c* = 15.01 Å [ref 16]

Atom	*x*	*y*	*z*	Wyckoff position
Au1	0	0	0.0000	3*a*
Ag1	0	0	0.6580	3*a*
Cu1	0	0	0.3260	3*a*
C1	0	0	0.1301	3*a*
C2	0	0	0.5218	3*a*
C3	0	0	0.8699	3*a*
N1	0	0	0.2058	3*a*
N2	0	0	0.4461	3*a*
N3	0	0	0.7942	3*a*

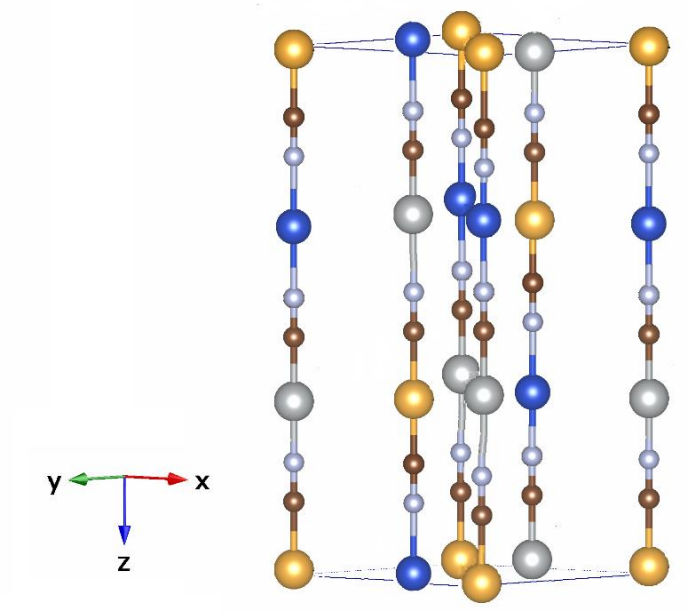

Figure S6. Model L. Key: Au atoms, yellow spheres; Ag atoms, silver spheres; Cu atoms, blue spheres; C atoms, brown spheres and N atoms, gray spheres.

Table S16. Model M

The *Pmm*2 model for $(Cu_{1/3}Ag_{1/3}Au_{1/3})CN$ at 100 K with $[Cu–NC–Ag–NC–Au–CN]_n$ ordered chains and mixed Cu-Au layers
Orthorhombic unit cell: *a* = 3.39, *b* = 5.87, *c* = 15.01 Å [ref 16]

Atom	*x*	*y*	*z*	Wyckoff position
Au1	0	0	0	1*a*
Au2	1/2	1/2	0.3260	3*c*
Ag1	0	0	0.6580	1*a*
Ag2	1/2	1/2	0.6680	3*c*
Cu1	0	0	0.3260	1*a*
Cu2	1/2	1/2	0.0000	3*c*
C1	0	0	0.1301	1*a*
C2	0	0	0.5218	1*a*
C3	0	0	0.8699	1*a*
C4	1/2	1/2	0.1958	3*c*
C5	1/2	1/2	0.4561	3*c*
C6	1/2	1/2	0.8042	3*c*
N1	0	0	0.2058	1*a*
N2	0	0	0.4461	1*a*
N3	0	0	0.7942	1*a*
N4	1/2	1/2	0.1201	3*c*
N5	1/2	1/2	0.5318	3*c*
N6	1/2	1/2	0.8799	3*c*

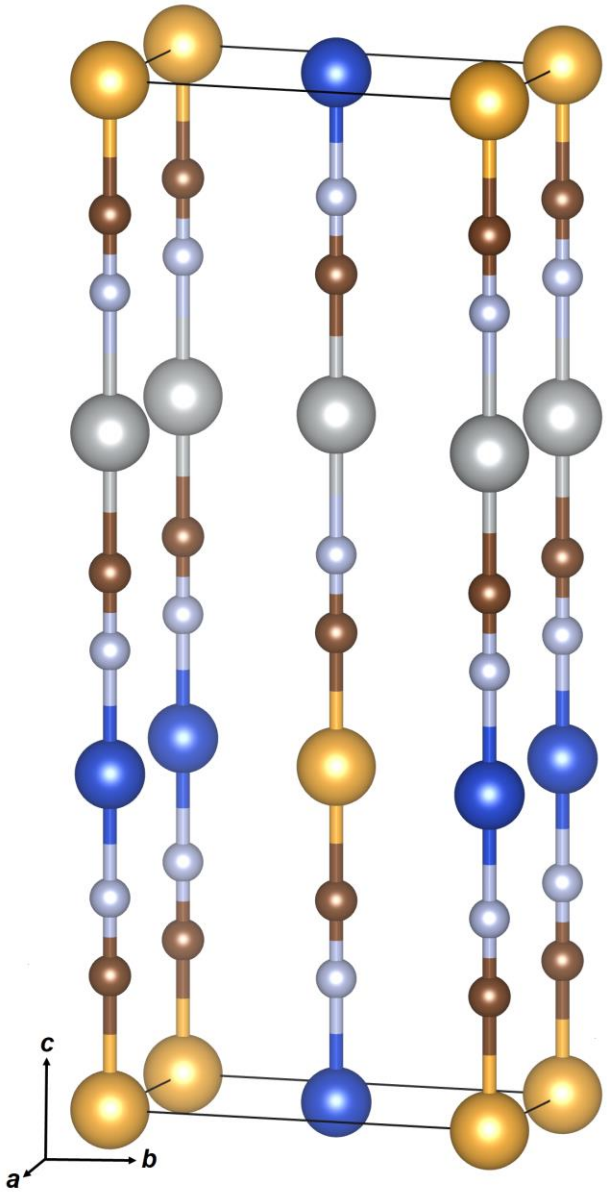

Figure S7. Model M. Key: Au atoms, yellow spheres; Ag atoms, silver spheres; Cu atoms, blue spheres; C atoms, brown spheres and N atoms, gray spheres.

Table S17. Model N
The *Pmm*2 model for $(Cu_{1/3}Ag_{1/3}Au_{1/3})CN$ at 100 K with $[Cu–NC–Ag–NC–Au–CN]_n$ ordered chains and mixed Ag-Au layers
Orthorhombic unit cell: *a* = 3.39, *b* = 5.87, *c* = 15.01 Å [this work]

Atom	*x*	*y*	*z*	Wyckoff position
Au1	0	0	0	1*a*
Au2	1/2	1/2	0.3420	3*c*
Ag1	0	0	0.3420	1*a*
Ag2	1/2	1/2	0	3*c*
Cu1	0	0	0.6740	1*a*
Cu2	1/2	1/2	0.6680	3*c*
C1	0	0	0.1301	1*a*
C2	0	0	0.4780	1*a*
C3	0	0	0.8699	1*a*
C4	1/2	1/2	0.2120	3*c*
C5	1/2	1/2	0.4720	3*c*
C6	1/2	1/2	0.8640	3*c*
N1	0	0	0.2058	1*a*
N2	0	0	0.5540	1*a*
N3	0	0	0.7942	1*a*
N4	1/2	1/2	0.1360	3*c*
N5	1/2	1/2	0.5480	3*c*
N6	1/2	1/2	0.7880	3*c*

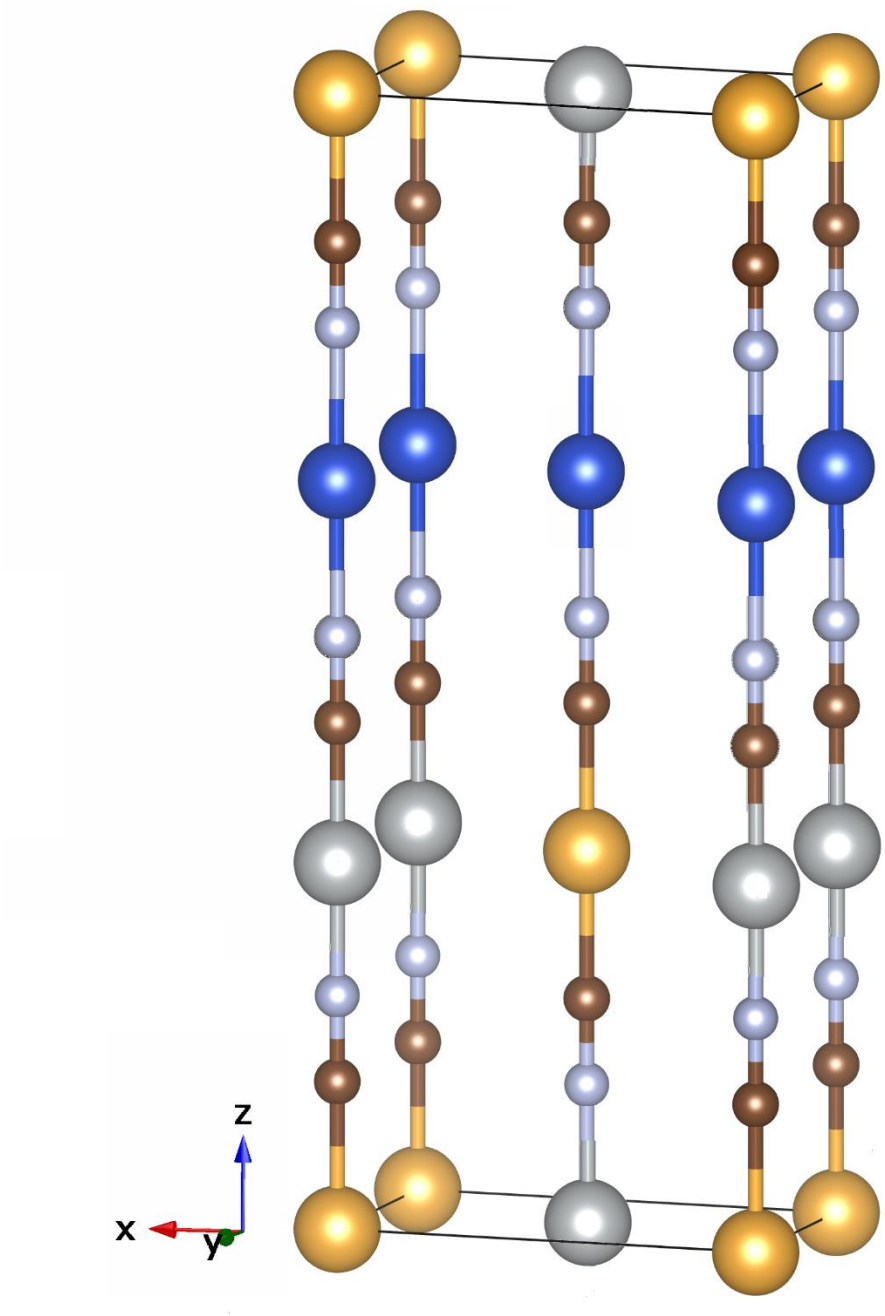

Figure S8. Model N. Key: Au atoms, yellow spheres; Ag atoms, silver spheres; Cu atoms, blue spheres; C atoms, brown spheres and N atoms, gray spheres.

S.7. Additional XPDF fits for $(Cu_{1/2}Au_{1/2})CN$ and $(Ag_{1/2}Au_{1/2})CN$

(a)$(Cu_{1/2}Au_{1/2})CN$ in Model (I) *Amam*{8}

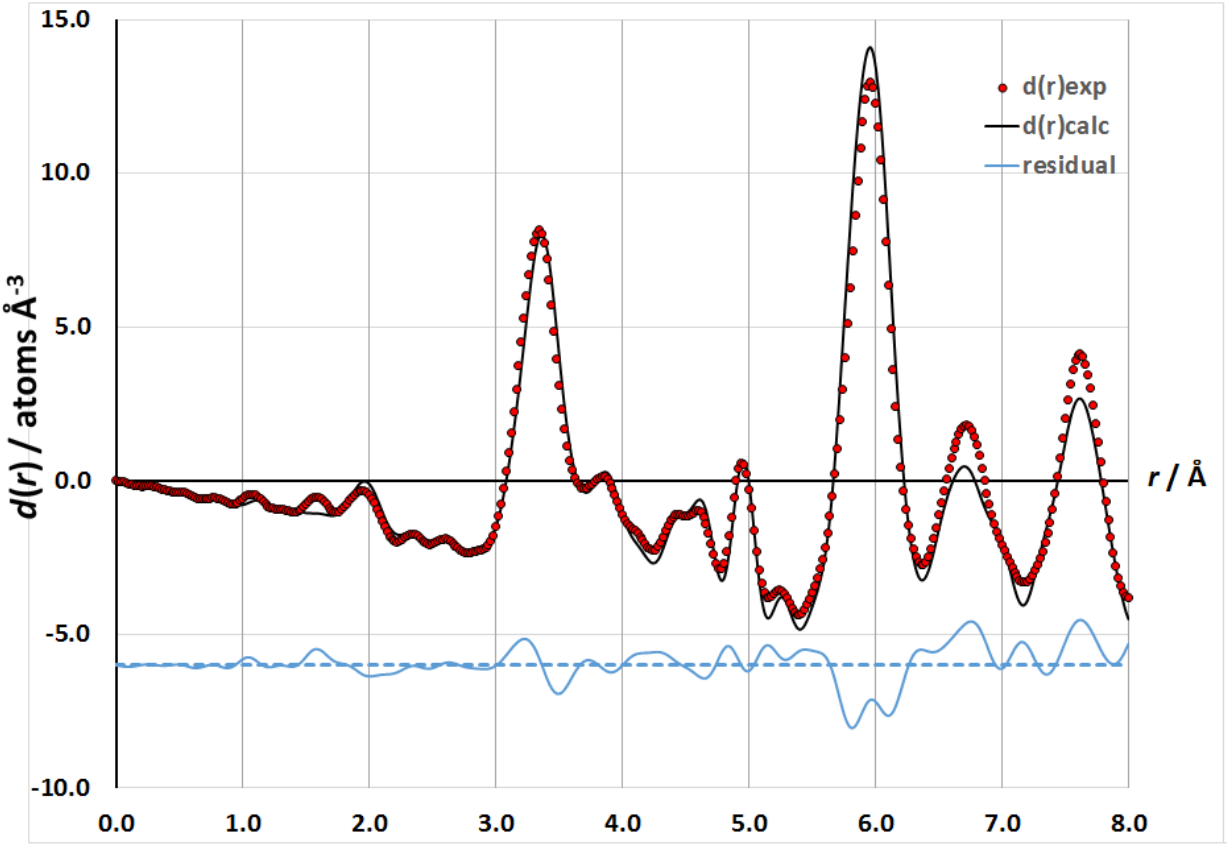

Figure S9. *D*(*r*) for $(Cu_{1/2}Au_{1/2})CN$ at 100 K and fit over the range ranges *r* = 0.0 – 8.0 Å using Model (**I**) in *Amam*{8}[R_{Dr}(0.0 – 8.0 Å) = 0.1896]. **(See Table S10.).**

Note: R factor, R_{Dr}, calculated using the following:

$$R_{D(r)} = \left[\sum |Y_i(obs) - Y_i(calc)|^2 / Y_i(obs)^2\right]^{1/2}$$

(b) ($Ag_{1/2}Au_{1/2}$)CN in Model (G) *I mmm*{4}, Model (I) *Amam*{8} and Model (J) *P6/mmm*{6}

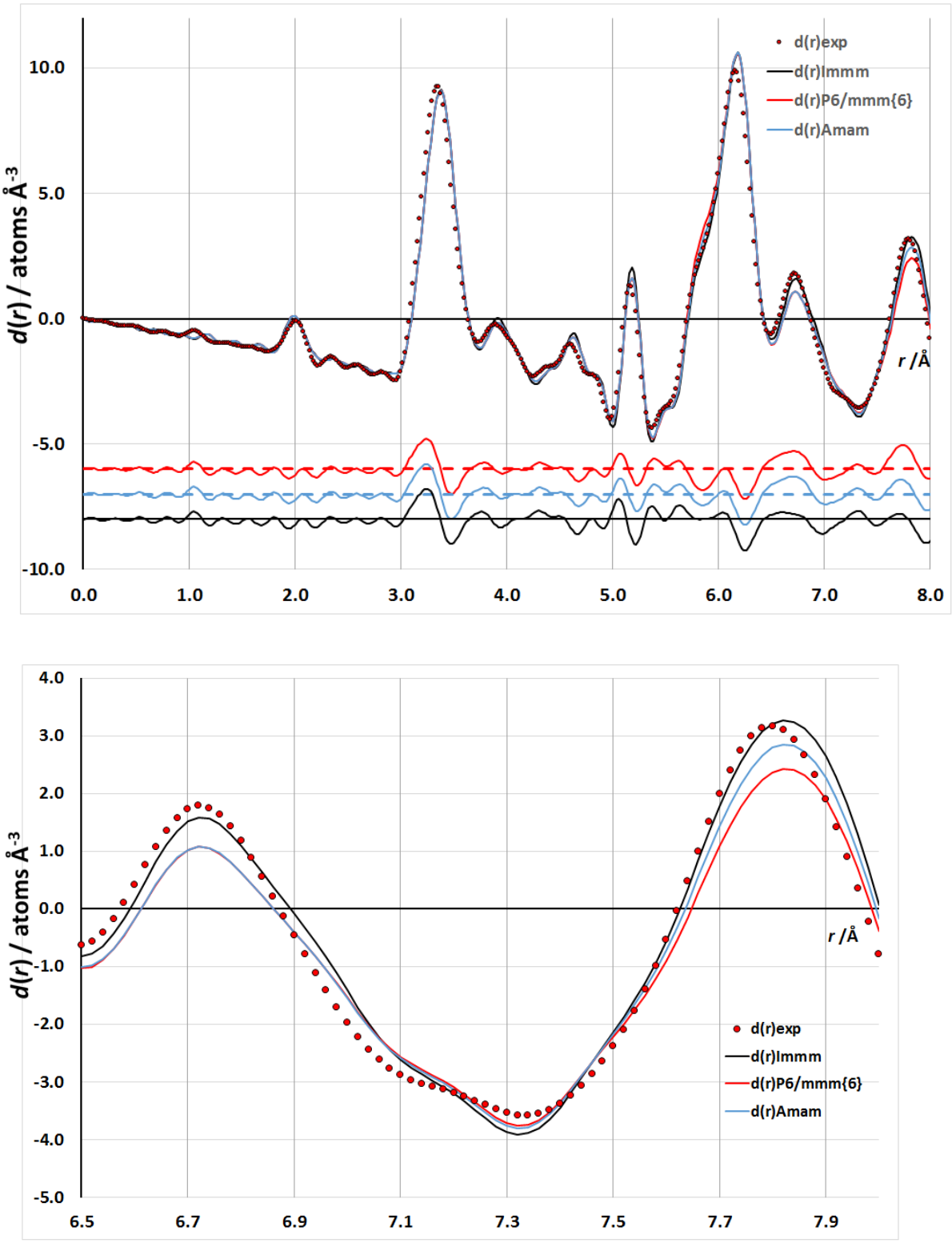

Figure S10. *D*(*r*) for ($Ag_{1/2}Au_{1/2}$)CN at 100 K and fits over the ranges *r* = 0.0 – 8.0 and *r* = 6.5 – 8.0 Å using (i) Model (**G**) *Immm*{4} [R_{Dr}(0.0 – 8.0 Å) = 0.1288 and R_{Dr}(6.5 – 8.0 Å) =

0.1619] (black line), (ii) Model (**I**) *Amam*{8} [R_{Dr}(0.0 – 8.0 Å) = 0.1261 and R_{Dr}(6.5 – 8.0 Å) = 0.1827] (blue line) and (iii) Model (**J**) *P6/mmm*{6} [R_{Dr}(0.0 –8.0 Å) = 0.1347 and R_{Dr}(6.5 – 8.0 Å) = 0.2111](red line). (**See Table S9.**).

Note: *R* factors, R_{Dr}, calculated using the following:

$$R_{D(r)} = \left[\sum |Y_i(obs) - Y_i(calc)|^2 / Y_i(obs)^2\right]^{1/2}$$

S.8. Solid-State NMR spectra

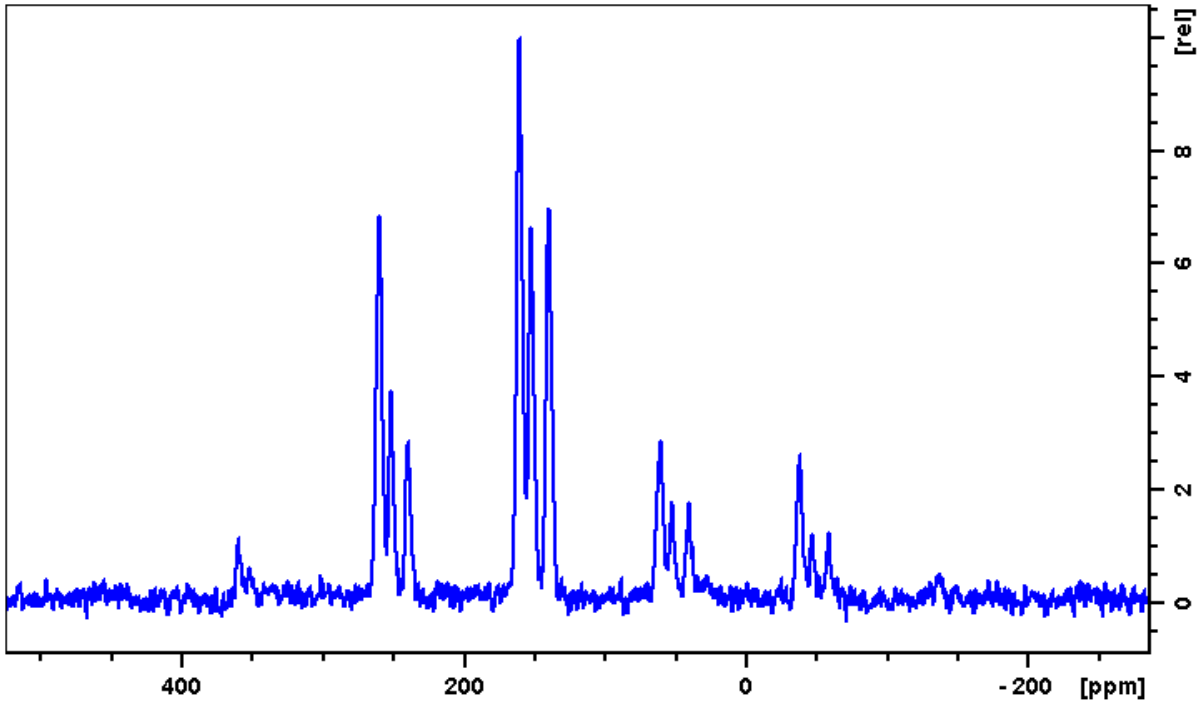

Figure S11. ^{13}C DEPTH spectrum of the High-Temperature form of CuCN spun at 10 kHz.

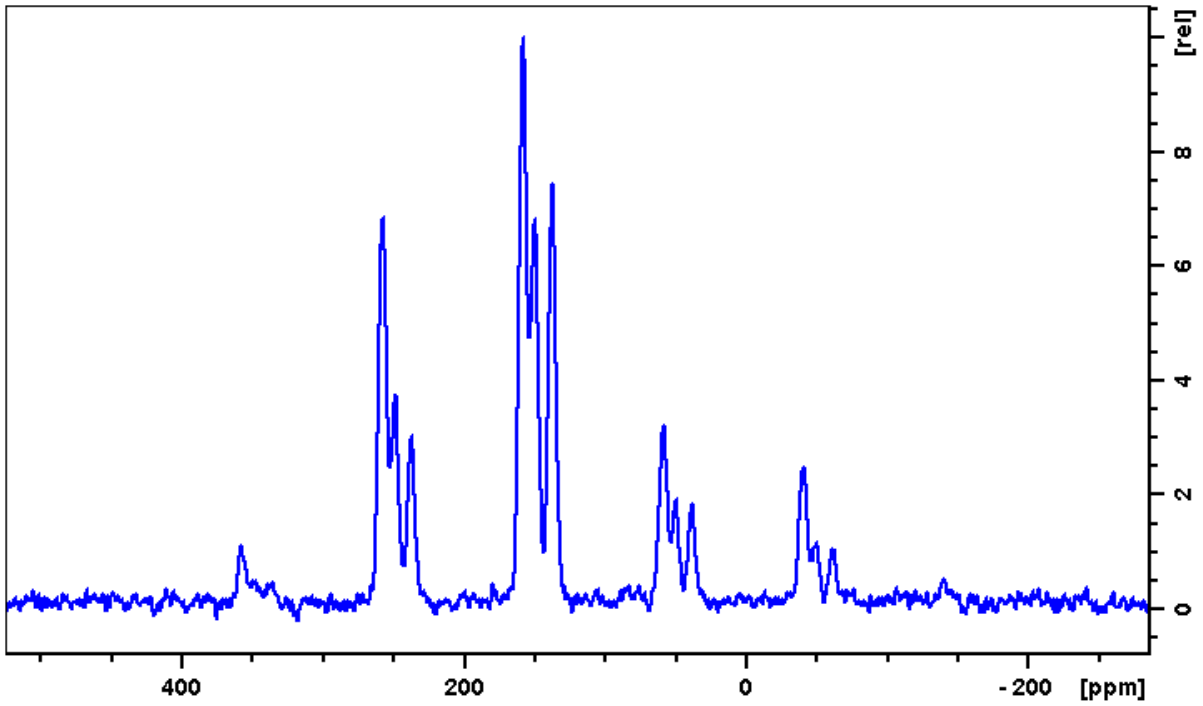

Figure S12. ^{13}C DEPTH spectrum of the Low-Temperature form of CuCN spun at 10 kHz.

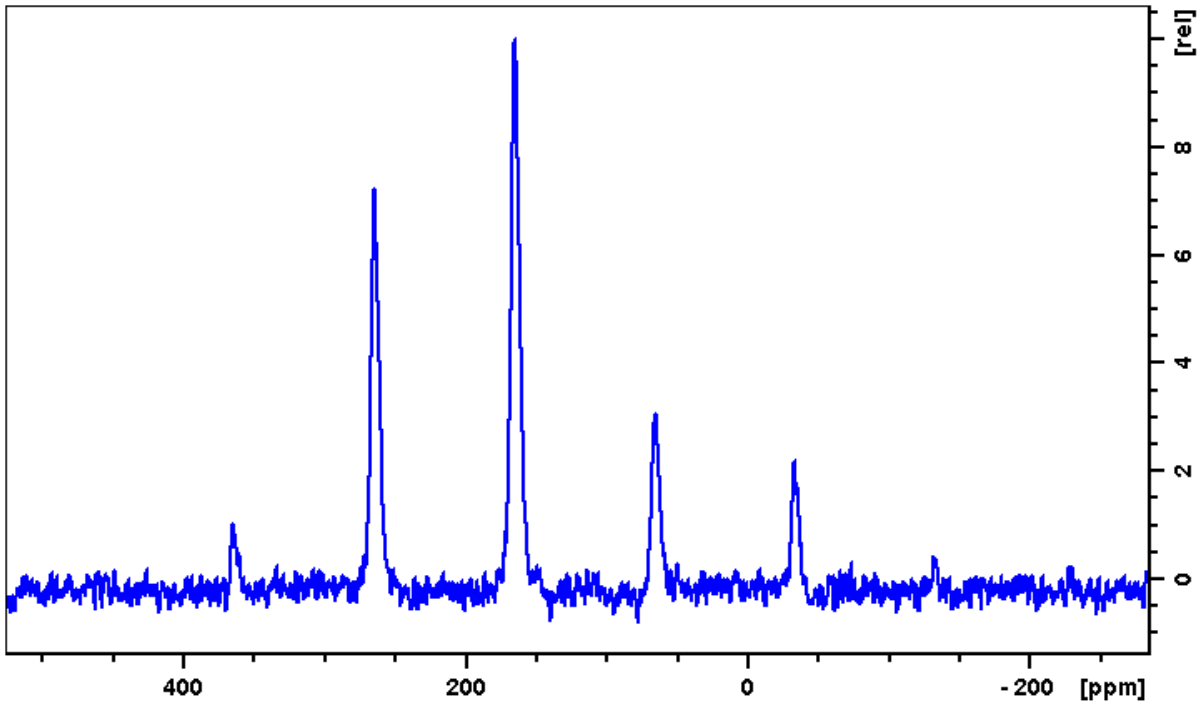

Figure S13. ^{13}C DEPTH spectrum of ($Cu_{½}Au_{½}$)CN spun at 10 kHz.

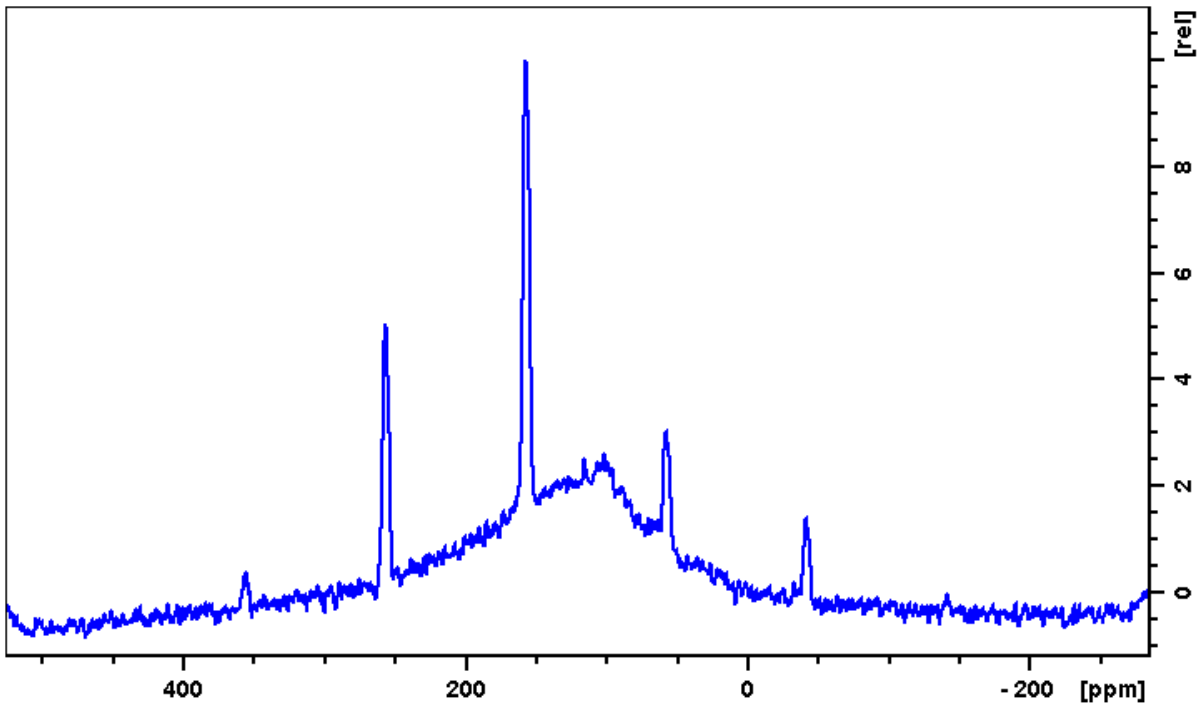

Figure S14. ^{13}C DPMAS spectrum of AgCN spun at 10 kHz.

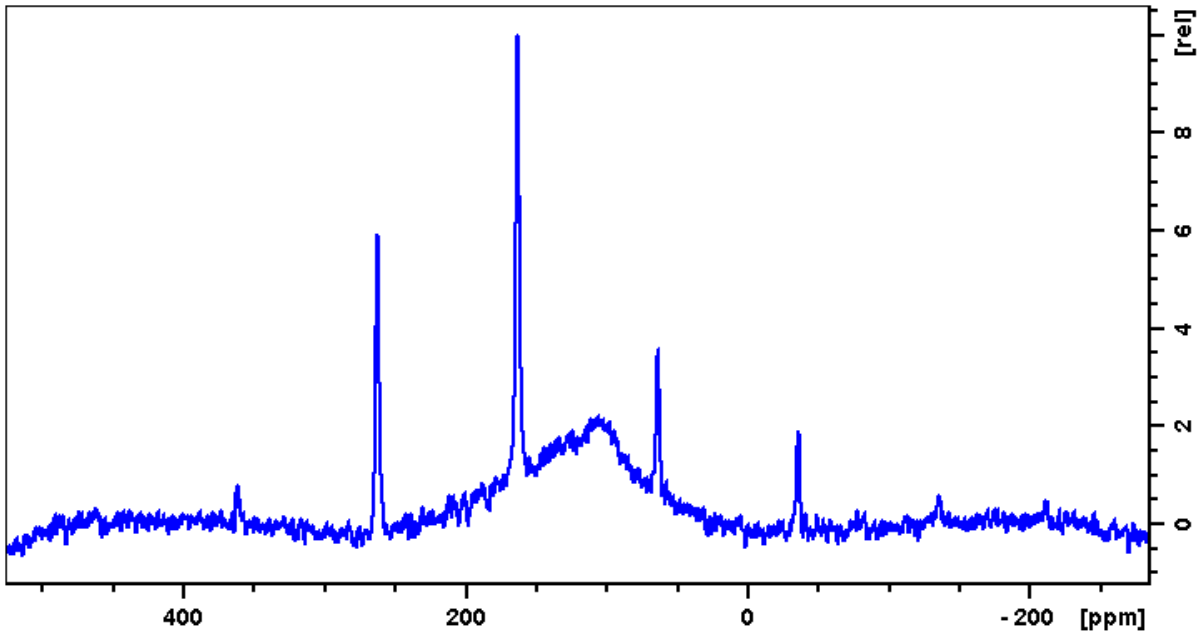

Figure S15. ^{13}C DPMAS spectrum of the $(Ag_{½}Au_{½})CN$ spun at 10 kHz.

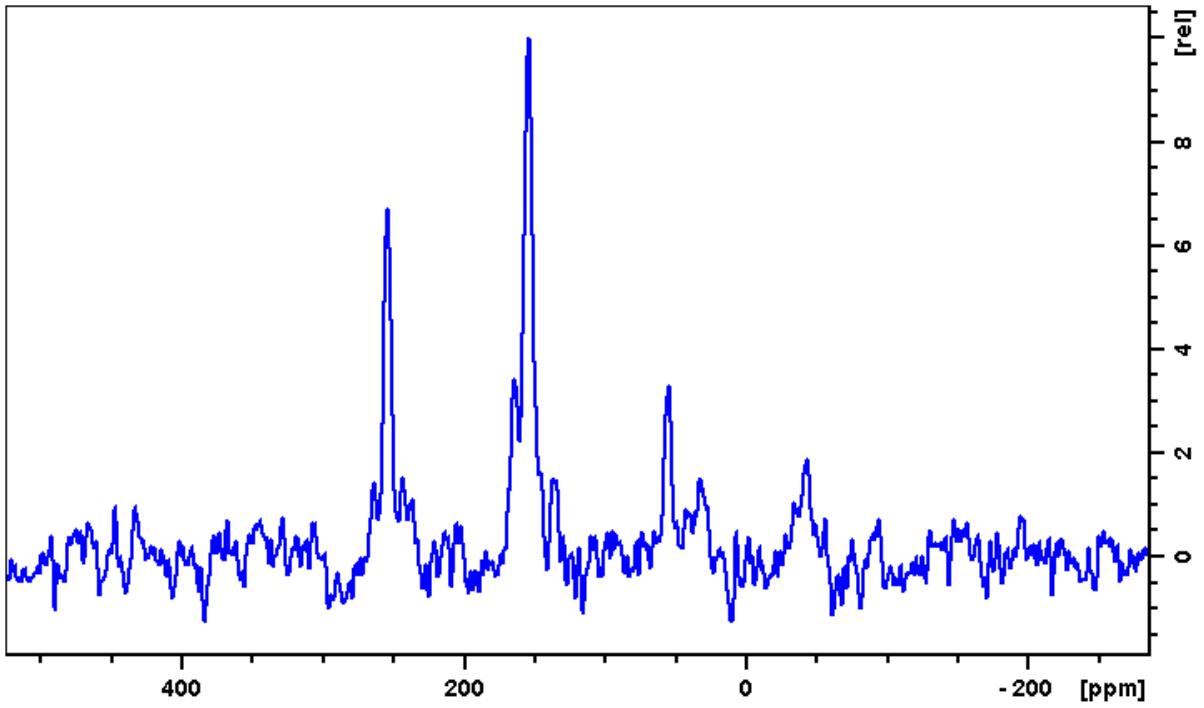

Figure S16. ^{13}C DEPTH spectrum of AuCN spun at 10 kHz.

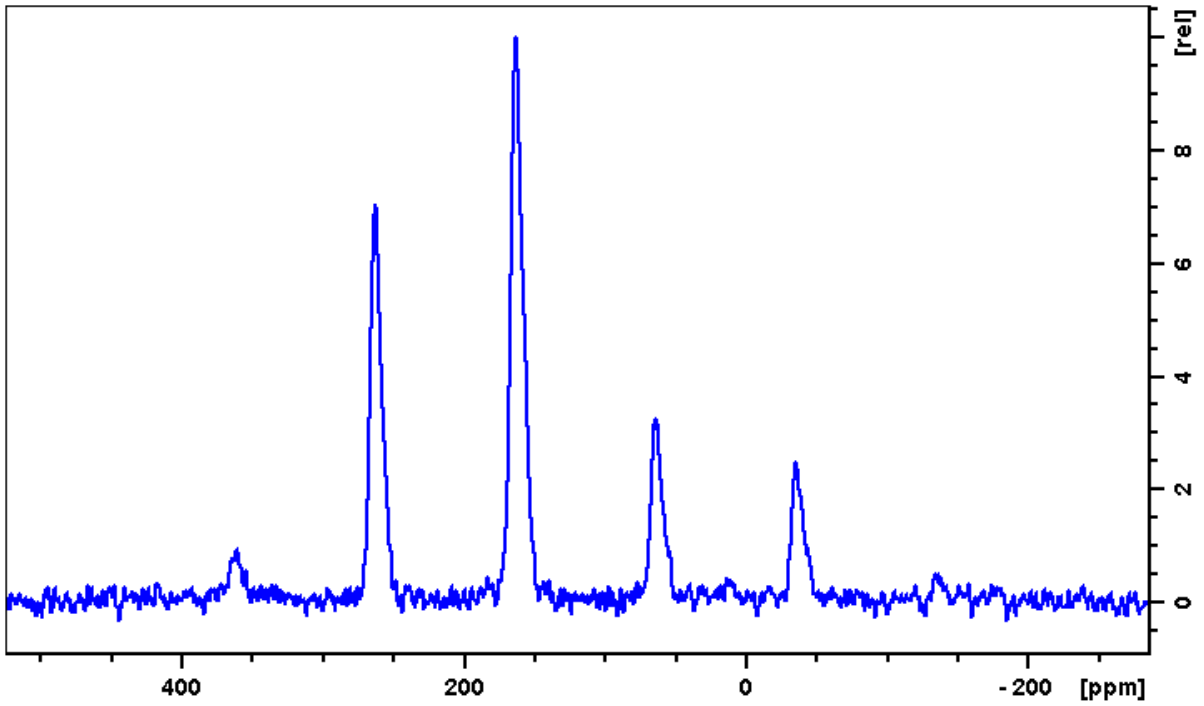

Figure S17. ^{13}C DEPTH spectrum of $(Cu_{⅓}Ag_{⅓}Au_{⅓})CN$ spun at 10 kHz.